Improving the 3D-CNS Organoid Model to Study Human Immunodeficiency Virus (HIV-1) Neuropathogenesis: Inclusion of the Blood-Brain Barrier

by

Aiyana-Mei Tom

B.S., West Virginia University, 2021

Submitted to the Graduate Faculty of the

School of Public Health in partial fulfillment

of the requirements for the degree of

Master of Science

University of Pittsburgh

2023

UNIVERSITY OF PITTSBURGH

SCHOOL OF PUBLIC HEALTH

This thesis was presented

by

Aiyana-Mei Tom

It was defended on

April 21, 2023

and approved by

Dr. William Brown Klimstra, Associate Professor, Dept. of Immunology

Dr. Jeremy Martinson, Assistant Professor, Dept. of Infectious Diseases and Microbiology

Thesis Advisor: Dr. Velpandi Ayyavoo, Professor, Dept. of Infectious Diseases and Microbiology

Improving the 3D-CNS Organoid Model to Study Human Immunodeficiency Virus (HIV-1) Neuropathogenesis: Inclusion of the Blood-Brain Barrier

Aiyana-Mei Tom, MS

University of Pittsburgh, 2023

The elimination of human immunodeficiency virus (HIV-1) from the body presents a challenge, even with the advent of effective antiretroviral therapy (ART). Although ART successfully manages HIV-1 infection, it does not completely eliminate the viral reservoir from the body. Antiviral drugs are inefficient in crossing the blood-brain barrier (BBB) and are thus unable to suppress the viral reservoir of HIV-1 in the central nervous system (CNS). The blood-brain barrier is a critically important protective barrier that is involved in providing essential biologic, physiologic, and immunologic separation between the central nervous system (CNS) and the periphery. HIV-1-infected monocytes from the periphery cross the BBB and establish themselves in the CNS as perivascular macrophages within the first 14 days of HIV-1 infection, yet the exact method of transmigration is still unknown. Our laboratory is developing an *in vitro* HIV-1-CNS model to understand the role of different cell lineages including blood brain barrier endothelial cells. To determine how the HIV-1 target cell types that cross the BBB, and establish infection in CNS, first I assessed the viral replication kinetics using THP-1 monocytes and primary human monocytes. I then infected target cells with HIV-1-reporter viruses, allowed the cells to differentiate and determined the amount of infectious virus, p24 and RNA, both pre- and post-infection. I then determined how HIV-1-infected monocytes and macrophages cross the BBB and establish infection in the brain to better develop future antiviral drugs.

Table of Contents

List of Tables

List of Figures

Preface

First, I would like to thank Dr. Ayyavoo for allowing me to take on this project. Thanks to her wisdom, I was able to learn a plethora of new skills and techniques that will help start my new career in science.

I would also like to thank my family and friends, new and old, who have supported me throughout my entire academic career. Your unwavering support and faith in me have uplifted me through my darkest times and kept me going in my brightest moments. I hope I have made you all proud.

To my love, thank you for everything. You believed in me, even when I didn't. Thank you for allowing me to pursue my dreams, and for standing with me as this dream becomes reality. Without you, none of this would be possible. Here's to our new future together.

1.0 The Impact of HIV-1

Human Immunodeficiency virus (HIV-1) is a highly pathogenic retrovirus that infects humans and in advanced stages, can lead to the development of acquired immune deficiency syndrome (AIDS) (1). According to the World Health Organization (WHO), at the end of 2021 an estimated 38.4 million people were living with HIV-1 (PLWH), with an annual average of 1.5 million new infections and 650,000 deaths worldwide, with Africa accounting for two-thirds of the infected population (2)**.**

After initial infection, infected individuals experience flu-like symptoms including fever, headache, rash, and sore throat. As the infection progresses, the immune system begins to weaken, leading to new symptoms including chills, weight loss, nausea, and diarrhea. Without treatment, the risk of co-infections from other pathogens, such as bacterial and fungal infections, greatly increases, making it harder for the immune system to clear opportunistic infections (3).

Currently, there is no cure for HIV-1, however, there are a variety of antiretroviral therapy (ART) drugs that are highly effective in inhibiting HIV-1 replication and when used in combination and taken consistently, can lead to a prolonged life and the suppression of viral detection within infected individuals (4).

1.1 HIV-1 Biology

HIV-1 is a blood-borne pathogen, that can enter mucosal surfaces via sexual contact between individuals with detectable viral load, child delivery from an infected mother to the

newborn baby, and percutaneous inoculation i.e., sharing needles between individuals with a detectable viral load (5, 6). HIV-1 targets host immune cells, such as lymphocytes and macrophages, specifically $CD4^+$ T helper cells. These T cells can express one or both HIV-1-co-receptors, CCR5 and CXCR4. Upon entry, the single-stranded viral RNA is reverse transcribed into double-stranded viral DNA and integrates into the host chromosome, establishing a persistent infection. Viral DNA then undergoes transcription and translation, producing viral proteins that are necessary for the construction of HIV-1 virions (7, 8). Newly synthesized viral proteins and RNA are trafficked to the viral assembly site on the host cell membrane. Once assembled, virions bud out of the host cell, and mature infectious virions spread to other host cells beginning the cycle again (9). As infection progresses, high levels of HIV-1 replication occur in the gut-associated lymphoid tissues where the majority of susceptible memory T cells reside (4). HIV-1 causes severe infection in these lymphocytes which stimulates an intense inflammatory response, causing a drastic depletion in T cells leading to immunodeficiency and susceptibility to infections. The ability of the virus to systemically infect the host via the blood stream, as well as its ability to deplete T cells, creates a deadly combination that can cripple the host (10, 11).

Serological tests are used to screen for viral DNA. Antibody tests, like p24 enzyme-linked immunosorbent assay (ELISA), are used to rapidly detect viral p24 antigen, the most abundant HIV-1 protein essential for capsid assembly (12). Additionally, the number of $CD4^+$ T cells reveals the degree of immunodeficiency, as well as the stage of infection. People living with HIV-1 (PLWH) who have a $CD4^+$ T cell count of 200 or fewer per mm^3 have progressed to AIDS (13, 14). But thanks to the advancements in science, there are multiple ART drugs available that can restore $CD4^+$ T cell counts and decrease the viral load in the host periphery.

For PLWH, ART drugs are the best course of treatment to suppress viral load and ultimately, ensure longevity and quality of life. There are a multitude of ART drugs that target and block essential viral molecules, as well as specific stages of the viral life cycle, that are required for the successful replication and production of HIV-1. For example, Tenofovir and Lamivudine are nucleoside/nucleotide reverse transcriptase inhibitors (NRTI) approved by the FDA in 2001. NRTIs are manufactured as a prodrug, meaning it needs to enter the host cell and become phosphorylated before it is activated. NRTIs lack the 3'-hydroxyl group, usually attached to the deoxyribose sugar, which eliminates the progression of the viral DNA chain by preventing the formation of phosphodiester bonds and preventing incoming viral 5'-nucleoside triphosphates from attaching. Another example, Raltegravir approved by the FDA in 2007 and more recently, Cabotegravir approved in 2021, are integrase inhibitors. Integrase is responsible for catalyzing the integration of viral double stranded DNA into the host chromosome by ligating the 3' ends of the viral DNA into the host DNA through a process called strand transfer. Integrase inhibitors bind to the catalytic domain and block the strand transfer reaction (4, 15, 16). HIV-1 mutates frequently due to its low-fidelity polymerase, which contributes to genetic diversity. The high genetic variability amongst these thousands of circulating species can lead to drug resistance, which means treating HIV-1 with one type of antiretroviral drug is just not enough. By combining several of these potent target-specific drugs, $CD4^+$ T lymphocyte numbers increase, indicating host immune reconstitution that is sufficient enough to reverse the clinical effects of immunodeficiency, and the suppression of viral load to undetectable levels: Undetectable = Untransmissible (14, 17).

1.2 HIV-1 Associated Comorbidities

Although the development and deployment of combination antiretroviral therapy (cART) has changed HIV-1 diagnosis from a death sentence to a livable chronic disease, HIV-1 associated comorbidities are on the rise. Furthermore, many of these drugs are unable to penetrate the central nervous system (CNS) and are unable to suppress viral load, especially within the CNS compartment (18, 19). There is an estimated 20-50% of PLWH may experience a variety of neurocognitive dysfunctions associated with HIV-1 infection, more commonly known as HAND (20–22). HIV-1 associated neurocognitive diseases (HAND) can be divided into three categories: asymptomatic neurocognitive impairment (ANI), mild neurocognitive disorder (MND), and HIV-1-associated dementia (HAD). Individuals with ANI exhibit mild impairment in two or more cognitive areas, although it does not interfere with normal functioning. Individuals with MND exhibit mild to moderate impairment in two or more cognitive areas, resulting in the mild interference of normal daily functions. Lastly, HAD, which is very rarely seen in PLWH, is described as exhibiting moderate to severe cognitive deficits resulting in the substantial interference with everyday functions, preventing an individual from employment and the ability to live independently (23–25). Currently in the cART era, the prevalence for HAD has significantly decreased from 20% to 5% in PLWH, while the prevalence for the milder cases of HAND, ANI and MND, have increased to 30% and 20%, respectively (26). A comparative analysis by Heaton et al., evaluated PLWH and people who are HIV-1 seronegative from the pre- and post-cART era, and found that PLWH from the pre-cART era had a greater impairment in motor skills and cognitive functioning, whereas in the post-cART era PLWH exhibit impairments in the cortical area, affecting executive function and impairments in memory, specifically prospective memory (22, 27).

Although the symptoms of HAND do not appear until the much later stages of HIV-infection, there is evidence that HIV-1 enters the brain early in the acute infection, within two weeks of initial infection (24, 28). Once the virus enters the bloodstream, these virions infect monocytes that migrate across the blood-brain barrier (BBB) and enter the CNS to establish infection. These infected monocytes differentiate into perivascular macrophages that are capable of productive HIV-1 infection in the CNS (29, 30). These macrophages infect other CNS target cells, such as microglia and resident macrophages. These cell types in the CNS act as HIV-1 reservoirs, where the virus accumulates in vesicles, slowly disseminating viral DNA and proteins that contribute to the degradation of the CNS. Other CNS cells include astrocytes that can harbor HIV-1, but cannot support the production of infectious virus and HIV-1 replication, making them a poor target for therapeutics (31, 32). Because the use of cART extends the life of PLWH, the disease results in a longer chronic inflammatory state induced by the production of both, HIV-1 virions in the periphery and in the CNS. The chronic inflammatory state leads to the deterioration of the BBB and formation of HAND in the late stages of disease.

1.3 Blood-Brain Barrier

All organisms with a well-developed central nervous system (CNS) have a blood-brain barrier (BBB). The BBB is a protective, selectively permeable barrier that is essential in maintaining a precisely regulated microenvironment that protects the neural tissues from infectious agents and other cytotoxic molecules circulating in the periphery (33). The BBB is a multi-cellular unit that is comprised of different cell lineages, including endothelial cells, astrocytes, and pericytes (Fig. 1).

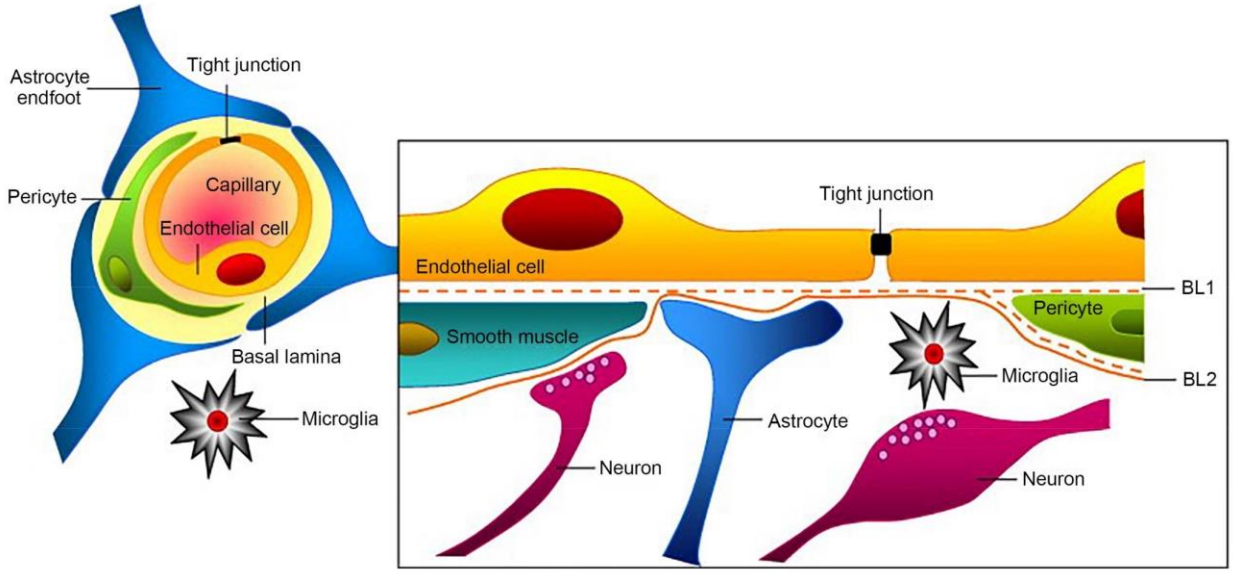

Figure 1. Multi-cellular blood-brain barrier. Depicted above are the cellular components of the blood-brain barrier including endothelial cells, tight junctions, astrocytes, pericytes, and microglia (Ref: He et al. 2018) (34).

1.3.1 Brain Microvascular Endothelial Cells

The BBB endothelial cells, also known as brain microvascular endothelial cells (BMECs), form the walls of blood vessels in contact with the brain (35). These unique endothelial cells found only in the brain, have specialized tight junctions (TJs) and adherens junctions (AJs) between each cell that are responsible for reducing the permeation of ions, large macromolecules and toxins via paracellular diffusion between endothelial cells from the periphery to the CNS (36, 37). In AJs, cadherin proteins make up the structural support of the cell and are anchored down to the cytoplasm via α-, β- and γ-catenin scaffolding proteins. TJs are also anchored down to the cytoplasm but by a different set of scaffolding proteins, ZO-1, ZO-2 and ZO-3, and are made up of occludins and claudins (38, 39). These BMECs also lack fenestrations – round transcellular pores found in the endothelium of organs where a higher rate of exchange between intra- and extravascular

compartments is required, such as endocrine tissue and GI mucosa. The lack of fenestrations also helps in preventing blood-borne pathogens from entering the CNS (40, 41). The highly selective nature of the BBB and the high energy demand of the brain create the need for nutrient transporters that facilitate the intake of various nutrients, including glucose, amino acids, and other nutrients needed for neuronal growth and function. Additionally, efflux pumps actively eliminate waste and toxic substances from the brain parenchyma (42–44). The BBB-specific endothelial cells make up the base of this intricate multi-cellular neurovascular unit.

1.3.2 Astrocytes

Astrocytes are CNS glial cells responsible for maintaining the homeostasis of the brain environment by providing nutrients to neurons and controlling the pH environment around the brain parenchyma (45). Astrocytes use their end feet to ensheath the entirety of the blood vessel, allowing for the uptake of nutrients as well as the control of blood flow by regulating the dilation and constriction of micro vessels (46, 47). Studies have shown that astrocytes can upregulate certain features of the BBB including, increased expression of efflux transporters and tighter TJs and AJs (43). Specifically, the secretion of laminins by the astrocytes are pertinent in maintaining BBB integrity, and their depletion leads to the reduction of TJ integrity within BMECs and a decreased expression of Aquaporin-4 (AQP4), whose function is to maintain water homeostasis within the CNS (48, 49). The main role of astrocytes is to support a healthy BBB by regulating and nourishing BMECs.

1.3.3 Pericytes

Pericytes, just like astrocytes, are responsible for maintaining the integrity of the BBB and the regulation of blood flow within the CNS (50). Pericytes are connective tissue cells that physically interact with BMECs, astrocytes and neurons to form gap junctions and allow for ions and nutrients to pass and strengthen the brain (51, 52). Recent studies have described two main functions of pericytes in the BBB: an increased expression of BBB-specific genes within BMECs, maintaining their differentiation, and inducing polarization of astrocyte endfeet around the CNS blood vessels, contributing to the regulation of cerebral blood flow (53). Although little is still known about pericytes, we do know their interaction with the rest of the BBB cells is needed to maintain a healthy brain environment.

1.3.4 Perivascular Macrophages

Perivascular macrophages (PVM) are a distinct population of myeloid cells with phagocytic function, located in the perivascular space surrounding blood vessels as they penetrate deep into the brain tissue (54). PVMs are elongated in shape, contain the surface markers CD163, CD206, and CD68, and are absent of smooth muscle actin and the microglial specific marker P2RY12, differentiating them from pericytes and microglia (55–57). The area postrema is a part of the brainstem that lacks tight junctions resulting in high BBB permeability. PVMs located in this region contribute to BBB integrity by isolating and preventing large proteins circulating in the periphery from penetrating the BBB by engulfing these unwanted molecules via phagocytosis (58). However, PVMs have been known to accumulate at damaged blood vessels after a BBB injury,

phagocytosing BMECs, indicating their ability to participate in BBB disruption under abnormal brain functioning (59).

1.3.5 Microglia

Microglial cells are small neuroglial cells located in the brain and spinal cord that are mesodermal in origin, differentiating them from neurons (60). They originate from erythromyeloid progenitor cells in the yolk sac during embryogenesis and develop the CNS, making them the main resident cells of the brain (61). They are known as the 'professional phagocytes' of the brain, recognizing cells that are about to undergo cell death within the CNS and eliminating them entirely (62). Upon activation, microglia become very mobile and rapidly make their way to the site of brain damage, releasing a plethora of cytokines, chemokines, and other neurotoxic proteins that contribute to neuroinflammatory effects of HAND (18, 63). Microglia cells are highly susceptible to HIV-1 infection, supporting the production of infectious virions via cell division, allowing HIV-1 to persist in the brain and become one of the main HIV-1 reservoirs in the CNS (64–66).

1.4 HIV-1 Infection of the Central Nervous System

Current research suggests that HIV-1 enters the brain within the first 14 days of acute infection (24, 67). Using the 'Trojan horse' model, HIV-1 enters the brain via infected peripheral blood monocytes or as free virion particles, both of which migrate across the BBB (29, 31, 68). As infected monocytes cross the BBB, they differentiate into perivascular macrophages and establish HIV-1 infection within the CNS, as illustrated in Figure 2 (69, 70). Peripheral blood monocytes

can be broken down into separate subpopulations, each with a distinct set of functions and surface markers.

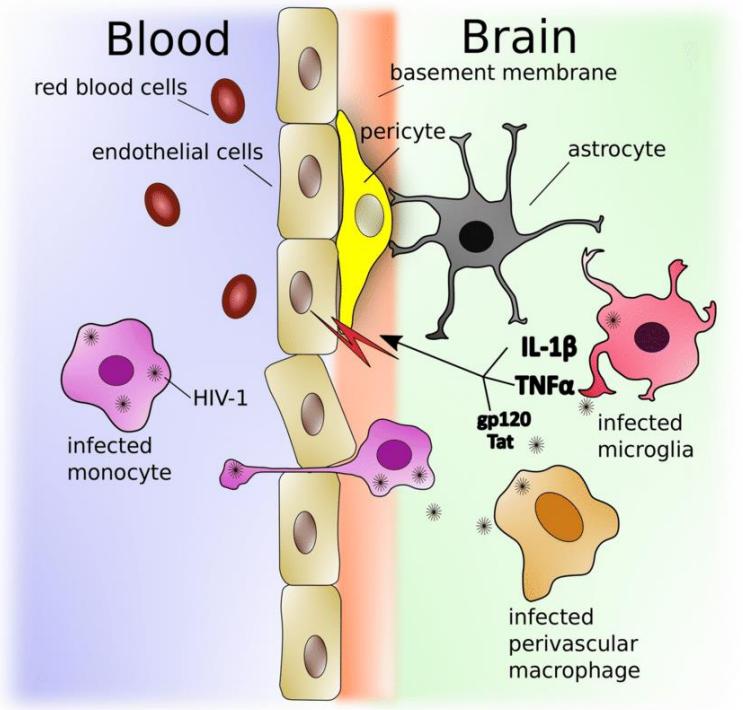

Figure 2. HIV-1-infected monocytes from the periphery crossing the blood-brain barrier into the CNS. The image above depicts entry of HIV-1 into the CNS via monocytes and free virions that cross the BBB. Infected micorglia release anti-inflammatory cytokines that damage the endothelial cells, allowing more infected monocytes to cross and establish themselves as perivascular macrophages in the CNS (Ref: Machado Andrade et al. 2019) (19).

Monocytes express two surface markers: CD14, the LPS receptor, and CD16, the $F_c\gamma$III receptor. About 90-95% of circulating monocytes within the periphery only express CD14 and are known as $CD14^+/CD16^-$ monocytes. About 5-10% of the circulating monocytes express both markers, CD14 and CD16 (71, 72). Upon HIV-1 infection, $CD14^+/CD16^+$ monocytes proliferate within the periphery and become highly permissible to HIV-1 infection (73). $CD14^+/CD16^+$ cells have been found in brain biopsy tissues of people who have succumbed to HIV-1-related illnesses,

allowing their use as predictive markers for cognitive decline in PLWH (74). During the course of HIV-1 infection, CCL2, a monocyte chemoattractant, is greatly increased in the CSF of PLWH who exhibit cognitive decline. The increased expression of CCR2 on monocytes indicates diseases characterized by chronic inflammation and increased trafficking of $CD14^+/CD16^+$ monocytes across the BBB to infiltrate the CNS.

Additionally, researchers have found that the process of monocyte transmigration across the BBB is also facilitated by the increased expression of multiple tight junction proteins and adhesion molecules on the surface of monocytes, specifically, junctional adhesion molecule-A (JAM-A), activated leukocyte cell adhesion molecule (ALCAM), platelet endothelial cell adhesion molecule 1 (PECAM-1), and CD99 (75–78). More importantly, JAM-A, ALCAM, and CCL2 directly impact transmigration of $CD14^+/CD16^+$ monocytes across the BBB, and when downregulated on the surface of endothelial cells, permit the migration of these infected monocytes from the periphery into the CNS (75). William et al. showed that $CD14^+/CD16^+$ monocytes that have been infected with HIV-1 at very low levels, can somehow maintain the upregulated expression of CCR2 on the surface and still produce an exuberant transmigration response to CCL2. This means that PLWH who are consistently taking their cART treatment can still become susceptible to neurocognitive impairment since viral load does not determine transmigration (79).

Once these HIV-1-infected $CD14^+/CD16^+$ monocytes cross into the CNS, HIV-1 persists in perivascular macrophages and microglial cells. Studies have shown that $CD68^+$ macrophages within the brain tissue of cART-treated, virologically suppressed individuals contain actively replicating HIV DNA and RNA, as well as the viral envelope protein gp120, the viral accessory protein Vpr, and the viral transcriptional activator Tat, providing evidence of an HIV-1

macrophage reservoir, causing ongoing neuroinflammation and severe neuronal damage that could possibly contribute to the development of HAND (80–84). While $CD4^+$ resting T cells are the major viral reservoir of HIV-1 infection, it is important to view the CNS as another potential HIV-1 viral reservoir. In some chronic HIV-1 infections, viral RNA can be found at higher concentrations in the CSF than in the blood, indicating a high amount of viral load in the brain and low amounts of antiretroviral drugs in the CNS.

Although there are ART drugs that have high CNS penetration effectiveness (CPE), a study found that these types of drugs failed to reduce the effect of neurocognitive performance disorder and instead functions declined or became worse. This prompted researchers to conclude that CPE cART regimens might actually be neurotoxic and enhance the persistence of HAND (20). Therapeutic strategies that aim to decrease the entry of HIV-1-infected $CD14^+CD16^+$ monocytes should target the surface markers JAM-A, ALCAM, and CCR2 to help eliminate viral reservoirs in the CNS and eradicate the symptoms of HAND. Thus, a better understanding of HIV-1 infection in the CNS is required to further develop therapeutics to target CNS reservoirs.

2.0 Specific Aims

Although antiretroviral therapy (ART) is effective in suppressing HIV-1 viral load from the periphery, these drugs are unable to cross over the blood-brain barrier (BBB) into the central nervous system (CNS) to eliminate viral reservoirs. The BBB is a highly selective protection barrier that is essential in maintaining homeostasis of the CNS. However, upon HIV-1 infection, infected monocytes from the periphery establish themselves in the CNS as HIV-1 viral targets/reservoirs, leading to the development of HIV-1 associated neurocognitive disorder (HAND). Since the exact mechanism of transmigration of infected monocytes across the BBB is still unknown due to the inability to study HIV-1 in the brain, our laboratory is developing an *in vitro* HIV-1-CNS model to understand the role of different cell lineages, including brain microvascular endothelial cells (BMECs). *I hypothesize that the integrity of the blood-brain barrier plays a role in transmigration of infected monocytes from the periphery to the CNS*. The hCMEC/D3 cell line will mimic the brain microvascular endothelial cells (BMECs) and create an in vitro blood-brain barrier. To test and validate my hypothesis, I propose the following aims using THP-1 monocytes and PMA-induced THP-1 macrophages:

<u>Aim 1:</u> Characterize HIV-1-virus infection in monocytes and macrophages *in vitro*.

A. Differentiate THP-1 monocytes to macrophage phenotype.
B. Generate viral stocks with and without VSV-G-Env for pseudotyping.
C. Standardize infection and measure viral kinetics in THP-1 monocytes and PMA-induced THP-1 macrophages.
D. Differentiate human primary monocytes to macrophage phenotype.

<u>Aim 2:</u> Understand the transmigration of infected monocytes and macrophages across the BBB *in vitro*.

A. Create the BBB by growing hCMEC/D3 brain endothelial cells in a Transwell® set up.

B. Study the transmigration of infected THP-1 monocytes and THP-1 macrophages across the BBB.

3.0 Materials and Methods

3.1 Cell Culture

HEK-293T, HMC3, and TZM-bl cells were cultured in DMEM (Gibco) containing 10% fetal bovine serum (Gibco), 1% (vol/vol) streptomycin/penicillin (Gibco), and 0.002% Plasmocin® (D10; InvivoGen), maintained at 37°C in 5% CO_2. THP-1 monocytes were similarly maintained and cultured in RPMI-1640 containing 10% fetal bovine serum, 1% streptomycin/penicillin, and 0.002% Plasmocin® (R10).

3.1.1 Differentiation of THP-1 Monocytes to Macrophages

THP-1 monocytes were differentiated with 10 ng/mL of phorbol 12-myristate 13-acetate (PMA; Millipore Sigma) (85, 86). THP-1 monocytes were seeded at 1.0 x 10^5 cells in R10 + PMA and incubated at 37°C in 5% CO_2 for overnight. The next day, culture media was removed, the cells washed with PBS and replaced with R10 culture media and rested for 72 hours.

3.1.2 Differentiation of Human Primary Monocytes to Macrophages

A frozen vial of peripheral blood mononuclear cells (PBMCs) was thawed in 37°C water bath for two minutes and centrifuged in a 15 mL conical tube containing culture media at 1200 rpm for five minutes, counted and washed for $CD14^+$ cell separation. CD14 microbeads (Miltenyi Biotec) and MACS buffer (PBS pH 7.2, 0.5% bovine serum albumin, 2 mM EDTA) were added

at a ratio of 20 μL:10 million cells and 80 μL:10 million cells, respectively, and incubated at 4°C for 15 minutes. $CD14^+$ cells were separated from PBMCs via MACS LS column and MACS magnet separator (Miltenyi Biotec). Isolated $CD14^+$ cells were counted, seeded at 3.0 x 10^5 cells per well in a 24-well tissue culture plate, and maintained in DMEM containing 10% fetal bovine serum, 1% streptomycin/penicillin, and 0.002% Plasmocin®.

The first half of the plate contained an additional 50 ng/mL sargramostin (granulocyte macrophage colony-stimulating factor [GM-CSF]; Sanofi) and 50 ng/μL filgrastim (macrophage colony-stimulating factor [M-CSF]; Amgen Inc.) to differentiate $CD14^+$ monocytes for seven days prior to infection. Media and growth factors were replenished every three days. The second half of the plate rested for 24 hours prior to infection.

3.1.3 Blood-Brain Barrier Cells

hCMEC/D3 (Millipore Sigma) cells were cultured in EndoGRO™-MV complete media (0.2% EndoGRO-LS Supplement, 5 ng/mL rh EGF, 10 mM L-Glutamine, 1.0 μg/mL hydrocortisone hemisuccinate, 0.75 U/mL heparan sulfate, 50 μg/mL ascorbic acid, 5% FBS; Millipore Sigma) supplemented with 1 ng/mL human recombinant fibroblast growth factor (FGF-2; Millipore Sigma). Collagen Type I, Rat Tail (Millipore Sigma) was thawed and diluted 1:20 in 1X PBS (Corning). 10 mL was used to coat a T75 flask and incubated at 37°C in 5% CO_2 for one hour. hCMEC/D3 cells were thawed and centrifuged at 300 x g for 3 minutes, supernatant discarded, and resuspended in culture media. The collagen coating was aspirated from the flask and the cell solution plated and maintained at 37°C in 5% CO_2.

3.2 Plasmid (Proviral) Preparation

One liter of LB Broth was made by adding 5 g of bacto-tryptone (BD Biosciences), 5 g of sodium chloride (Fisher Scientific), 2.5 g of bacto-yeast (BD Biosciences) in 475 mL of distilled water and autoclaved for 20 minutes. In a one-liter Erlenmeyer flask, ampicillin (Sigma Aldrich) was diluted 1 μL:1 mL in LB broth (40 μL of ampicillin in 40 mL of LB broth). A small sample of the frozen glycerol stock labeled pNL(YU-2)EGFP was collected via micropipette tip and dropped into the Erlenmeyer flask, which shook overnight at 3000 rpm in 30°C.

The next day, the sample turbidity was assessed and prepared for plasmid DNA purification via GeneJET Plasmid Maxi Prep Kit (Thermo Scientific). The bacterial culture was centrifuged at 5000 x g for 10 minutes, the supernatant discarded, and the pellet resuspended in 6 mL of resuspension solution. Once the pellet was completely broken up, 6 mL of lysis solution was added and gently mixed by inverting five times and incubating for three minutes at room temperature. 6 mL of neutralization solution was added and mixed by inverting seven times. 0.8 mL of endotoxin binding reagent was also added and inverted seven times then incubated at room temperature for five minutes.

Next, the solution was centrifuged for 20 minutes at 48000 x g to remove cell debris and chromosomal DNA. The supernatant containing the plasmid DNA was transferred to a new 50 mL conical tube and an equal part of 96% ethanol was added. The lysate was centrifuged at 2000 x g for three minutes in a purification column with the flow-through discarded. After, 8 mL of wash solution I (with isopropanol) was added to the purification column, centrifuged for two minutes at 3000 x g, with the flow-through discarded, and 8 mL of wash solution II (with ethanol) was added to the purification column, centrifuged for two minutes at 3000 x g, with the flow-through

discarded. The wash solution II step was repeated again, followed by another round of centrifugation at 3000 x g for five minutes, with flow-through and collection tube discarded.

Finally, the purification column containing the plasmid DNA was eluted with 500 μL of autoclave water, and DNA concentration and purity was assessed via NanoDrop™ 2000/2000c spectrophotometer and analysis software (Thermo Fisher).

3.3 Virus Production and Titration

3.3.1 Pseudotyping HIV-1 Virus Particles

HEK293T cells were transfected by seeding 1.5 x 10^6 cells in 7 mL of culture media on 10 cm^2 tissue culture dishes and grown overnight to 80% confluency. One plate of cells was transfected with VSV-G-Env, that included 4 μg of proviral DNA + 1 μg of VSV-G-Env, and the other plate was absent of VSV-G-Env containing 5 μg of plasmid DNA, along with 15 μL of PolyJet™ (SignaGen) diluted in 500 μL of DMEM, which was then added dropwise to each plate. 16 hours post-transfection, the media was removed from each plate and the cells washed with PBS and replaced by 11 mL of culture media and incubated at 37°C in 5% CO_2 for 48 hours. Supernatants were harvested from each dish and centrifuged at 1000 rpm for five minutes and purified through a 0.45 μm filter (Millipore Sigma) to remove cell debris.

3.3.2 Viral Titration

Viral titers were assessed via TZM-bl assay using the transfected supernatants. 5.0 x 10^3 TZM-bl cells were seeded in triplicate in a 96-well plate and grown overnight to 80% confluency. The cells were infected with 1:100, 1:10, 1:2, and undiluted quantities of virus and incubated for 48 hours. The infected cells were washed, fixed, and stained with 1X DAPI for 5 minutes. The stained cells were then counted: when looking for optimal concentration, each well should contain a countable number of cells, between 50 and 150 cells stained, per well. Once the optimal concentration was found, each replicate was counted and averaged to yield the measure of infectivity in infectious particles per milliliter (IP/mL) using the following equation:

$$\frac{IP}{mL} = average\ eGFP^{+}\ \text{cells} * \text{dilution factor} * 1000$$

3.4 Viral Infections and Replication Kinetics

3.4.1 THP-1 Monocyte Infections

THP-1 monocytes constitutively expressing mCherry were seeded at 1.0 x 10^5 cells per well in a 12-well plate and separately infected with pNL(YU-2)EGFP, pNL(YU-2)EGFP + VSV-G-Env, pNL(BaL)iRFP, and pNL(BaL)iRFP + VSV-G-Env, at an MOI of 0.5 and 1.0, and incubated for 48 hours at 37°C in 5% CO_2. Fluorescent cells were visualized with the EVOS™ M5000 microscope (Thermo Fisher).

THP-1 monocytes were seeded at 5.0 x 10^5 cells per well in a 12-well plate and infected with pNL(YU-2)EGFP + VSV-G-Env and pNL(BaL)iRFP + VSV-G-Env at an MOI of 0.5 and

1.0 and incubated for 48 hours at 37°C in 5% CO_2. Fluorescent cells were visualized with the EVOS^{TM} M5000 microscope (Thermo Fisher).

The first half of the plate was differentiated with 10 ng/mL of phorbol 12-myristate 13-acetate (PMA; Millipore Sigma) and incubated for 24 hours, washed with PBS, and replenished with fresh culture media. Supernatant was collected on day 1, 3, 5, 7 and 9. 10 days post-infection, 1 μg/mL LPS was added to each well and incubated for 16 hours. Finally, the infected THP-1 monocytes were centrifuged at 1600 rpm for 5 minutes, and the supernatant and pellet collected for cytokine analyses. The infected PMA-induced THP-1 macrophages supernatant was collected, the cells trypsinized with 0.05% trypsin EDTA for five minutes and centrifuged at 1600 rpm for five minutes, and the cell pellet collected for cytokine analyses.

3.5 p24 Enzyme-Linked Immunosorbent Assay (ELISA) Quantification

Harvested supernatant from infected THP-1 monocytes and PMA-induced THP-1 macrophages were evaluated for HIV-1 p24 capsid protein production using HIV-1 p24^{CA} antigen capture assay kit (Leidos).

3.5.1 Plate Preparation

100 μL of capture antibody diluted 1:300 in DPBS (Quality Biological) mixed for 30 minutes and then added to each well of a 96-well high binding ELISA plate (Corning) and incubated overnight at 4°C. The capture antibody was aspirated from the plate and patted dry on clean paper towels. 300 μL of blocking solution (1% BSA in DPBS) was added to each well and

incubated for one hour at room temperature. Next, the blocking solution was aspirated from each well in the plate and washed with wash buffer (0.05% Tween®20 in PBS) five times using the 405 LS microplate washer (BioTek). The plate was then rotated 180°, washed an additional five times, and thoroughly patted dry on clean paper towels.

3.5.2 Assay Procedure

Standards were created via serial dilution of p24 HIV-1 standard reagent (Leidos) and sample diluent (1% BSA, 0.002% Tween®20 in RPMI-1640, 0.45 μm filter sterilized). 100 μL of standards and sample was added to each respective well and incubated for two hours at 37°C in 5% CO_2. The plate was washed and dried as previously described, and 100 μL of primary antibody diluted 1:300 with primary antibody diluent (1% fetal bovine serum, 0.02% normal mouse serum in RPMI-1640, 0.45 μm filter sterilized) was added to each well and incubated for one hour at 37°C in 5% CO_2. The plate was washed and dried thoroughly, as previously described, then 100 μL of secondary antibody diluted 1:800 in secondary antibody diluent (1% Tween®20, 0.05% normal goat serum, 0.02% normal mouse serum in RPMI-1640, 0.45 μm filter sterilized) was added to each well and incubated for one hour at 37°C in 5% CO_2. For a final time, the plate is washed and thoroughly dried, as previously described, and 100 μL of tetramethylbenzidine (TMB) peroxidase substrate (SeraCare) added to each well and incubated at room temperature for 25 minutes. At this point, the color of the wells turned blue, with higher concentrations of p24 showing a deeper blue color. Immediately after 25 minutes, 100 μL of 1N HCl (37% HCl in distilled water) was added to each well to stop the reaction; upon addition, each well became bright yellow in color. Optical density was measured using the SpectraMax Plus 384 Microplate reader

(Molecular Devices) set at 450 nm and the SoftMax Pro 6 analysis software (Molecular Devices). Standard curves were produced using known concentrations and experimental absorbances. Linear trend lines were used to create an equation for calculating viral protein amounts in picogram per milliliter (pg/mL).

3.6 Cytokine ELISA Quantification

Harvested supernatant from infected THP-1 monocytes and PMA-induced THP-1 macrophages were evaluated for TNF-α and IL-1β production using Human TNF-α DuoSet® ELISA kit (R&D Systems) and Human IL-1β/IL-1F2 DuoSet® ELISA kit (R&D Systems).

3.6.1 Plate Preparation

100 μL of capture antibody diluted to 4.0 μg/mL in PBS was added to each well of a 96-well high binding ELISA plate (Corning) and incubated overnight at room temperature. The capture antibody was aspirated from each well in the plate and washed with wash buffer (0.05% Tween®20 in PBS) three times using the 405 LS microplate washer (BioTek) and thoroughly patted dry on clean paper towels. 300 μL of blocking solution (1% BSA in DPBS) was added to each well and incubated at room temperature for one hour. After, the blocking solution was aspirated and washed as previously stated.

3.6.2 Assay Procedure

A seven-point standard curve for each cytokine standard was made and 100 μL was added to the 96-well plate, including 100 μL of each sample, and incubated at room temperature for two hours. The highest standard concentration was 1000 pg/mL for TNF-α, and 250 pg/mL for IL-1β. The plate was washed and thoroughly dried, as previously stated. Detection antibody was diluted 50 ng/mL for TNF-α and 75 ng/mL for IL-1β, and 100 μL added to their respective plates and incubated for two hours at room temperature. The plate was then washed and thoroughly dried, as previously stated. Streptavidin conjugated to horseradish-peroxidase (HRP) was diluted 1:40 in 1% BSA, then 100 μL added to each well and incubated for 20 minutes at room temperature. The plate was washed and thoroughly dried, as previously stated. 100 μL of tetramethylbenzidine (TMB) peroxidase substrate (SeraCare) was added to each well and incubated at room temperature for 20 minutes, resulted in an increase in color change. Immediately after 20 minutes, 1N HCl was added to each well to stop the reaction, where each well changed color from blue to yellow. Optical density was measured using the SpectraMax Plus 384 Microplate reader (Molecular Devices) at 450 nm and the SoftMax Pro 6 analysis software (Molecular Devices). Seven-point standard curves were produced using known concentrations and experimental absorbances. Linear trends were used to create an equation for calculating cytokine amounts in picogram per milliliter (pg/mL).

3.7 Quantitative Reverse Transcription Polymerase Chain Reaction (RT-qPCR)

HIV-infected THP-1 monocytes were collected and centrifuged at 1200 rpm for five minutes at 4°C. HIV-1-infected PMA-induced THP-1 macrophages were also collected via 0.05% trypsin EDTA (Gibco) and centrifuged at 1200 rpm for five minutes at 4°C. After centrifuging, supernatants were discarded, and the pellets kept at 4°C for mRNA quantification using the GeneJET RNA Purification Kit (Thermo Fisher), the Veriti^{TM} 96-well fast thermal cycler (Applied Biosystems), the ViiA 7 Real-Time PCR system (Applied Biosystems), and QuantStudio Real-Time PCR System (Applied Biosystems) software analysis. All of samples, the reagents, and the PCR plate were kept on ice to maintain a constant 4°C temperature.

3.7.1 RNA Extraction and Purification

Each pelleted sample was resuspended in 600 μL of lysis buffer supplemented with B-mercaptoethanol (Sigma Aldrich) and vortexed for 10 seconds, until the mixture is homogenized. After adding 360 μL of 96% ethanol to each sample, 700 μL of the lysate was then transferred to the GeneJET RNA Purification column inserted into a collection tube, then centrifuged at 12000 x g for one minute. The flow-through was discarded and the remaining lysate transferred to the purification for centrifugation and flow-through discarded. Next, 700 μL of wash buffer was added to each sample, centrifuged at 12000 x g for one minute, and flow-through discarded. An additional 600 μL of wash buffer was added to the column and the centrifuge step repeated and flow-through discarded. A final 250 μL of wash buffer was added to the column for a final centrifugation and the flow-through and collection tube are discarded, and the column transferred to a new sterile Eppendorf tube. 50 μL of nuclease free water was added to the center of the GeneJET column and

centrifuged at 12000 x g for one minute to elute the RNA. RNA concentration and purity was assessed via NanoDrop™ 2000/2000c spectrophotometer and analysis software (Thermo Fisher).

3.7.2 Construction of cDNA

cDNA was generated using the RNA isolated from the infected supernatants and the High-Capacity cDNA Reverse Transcription (RT) Kit (Applied Biosystems™). A 2X RT master mix was prepared, containing 2 µL 10X RT buffer, 0.8 µL 25X dNTP mix, 2 µL 10X RT random primers, 1 µL MultiScribeTM RT, and 4.2 µL nuclease free water. Each reaction tube received 1 µg RNA and nuclease free water was added to bring each reaction volume to 20 µL. Reaction tubes were mixed well and transferred to Veriti™ 96-well Thermal Cycler (Applied Biosystems™) under the condition in Table 1.

Table 1. cDNA conversion reaction specifications.

	Step 1	**Step 2**	**Step 3**	**Step 4**
Temperature (°C)	25	37	85	4
Time (minutes)	10	120	5	∞

3.7.3 RT-qPCR

A master mix containing, 3 µL cDNA, 8.75 µL TaqMan™ Master Mix II (Applied Biosystems), 0.875 µL TaqMan™ assay probes (Applied Biosystems) in nuclease free water, was created. The probes, GAG and GAPDH, were used in this experiment. Each sample was done in

triplicate, with 5 µL of the total reaction added to the corresponding well of a 384-well plate and sealed with a cover. Under the conditions in Figure 3, an amplification curve was produced via ViiA 7 Real-Time PCR system (Applied Biosystems), and QuantStudio Real-Time PCR System (Applied Biosystems) analysis software. Fold change was calculated by the comparative ΔΔCt method, with normalization to an appropriate endogenous control.

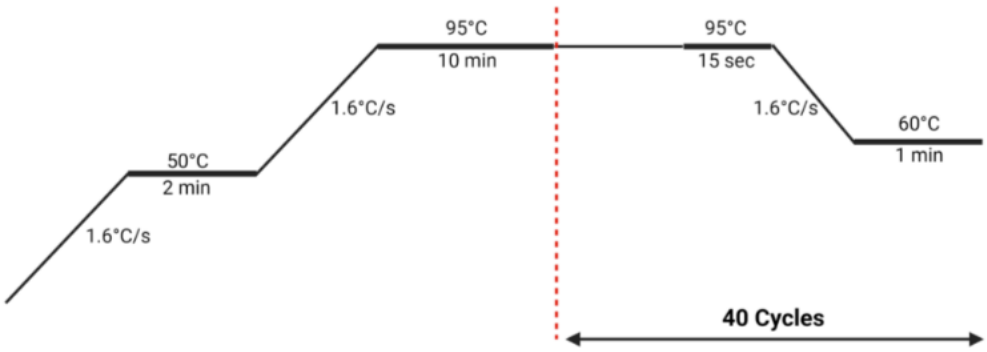

Figure 3. RT-qPCR reaction parameters.

3.8 Incorporation of the Blood-Brain Barrier

8.0 µm Transwell® (Corning) was coated with 100 µL Collagen Type 1, Rat Tail (Millipore Sigma) diluted 1:20 in PBS (Corning) and incubated at 37°C in 5% CO_2 for two hours. The collagen was aspirated and hCMEC/D3 (Millipore Sigma) cells were seeded at 6.8 x 10^3 cells in 100 µL of EndoGRO™-MV complete media (Millipore Sigma) on each Transwell®. The Transwell® was placed in a 24-well containing 1 mL of hCMEC/D3 culture media and incubated at 37°C in 5% CO_2 for 24 hours. After incubation, 500 µL of hCMEC/D3 culture media in each well was removed and replaced with 500 µL of R10. THP-1 monocytes separately infected with

pNL(YU-2)EGFP and pNL(BaL)iRFP at an MOI = 0.2, were counted and added to each corresponding Transwell®. After 48 hours, each Transwell® was removed and the amount of infected and non-infected monocytes were counted in each well.

4.0 Results

4.1 Aim 1: Characterize HIV-1-Virus Infection in Monocytes and Macrophages *in vitro*.

4.1.1 Differentiation of Macrophages from THP-1 Monocytes Using Phorbol 12-myristate 13-acetate (PMA)

To generate macrophages, PMA-induced differentiation of THP-1 monocytes, was performed to determine optimal concentration. Three different concentrations of PMA were selected and tested (85). THP-1 monocytes were seeded in separate wells with various concentrations of PMA for 24 hours, then rested in fresh culture media for an additional 72 hours (Fig. 4A). Results indicated 10.0 ng/mL of PMA was sufficient to induce adherent cells, with spindle-like, stellate morphology (Fig. 4B, white arrows). Based on these results, 10.0 ng/mL was selected for future infection assays using differentiated THP-1 monocytes.

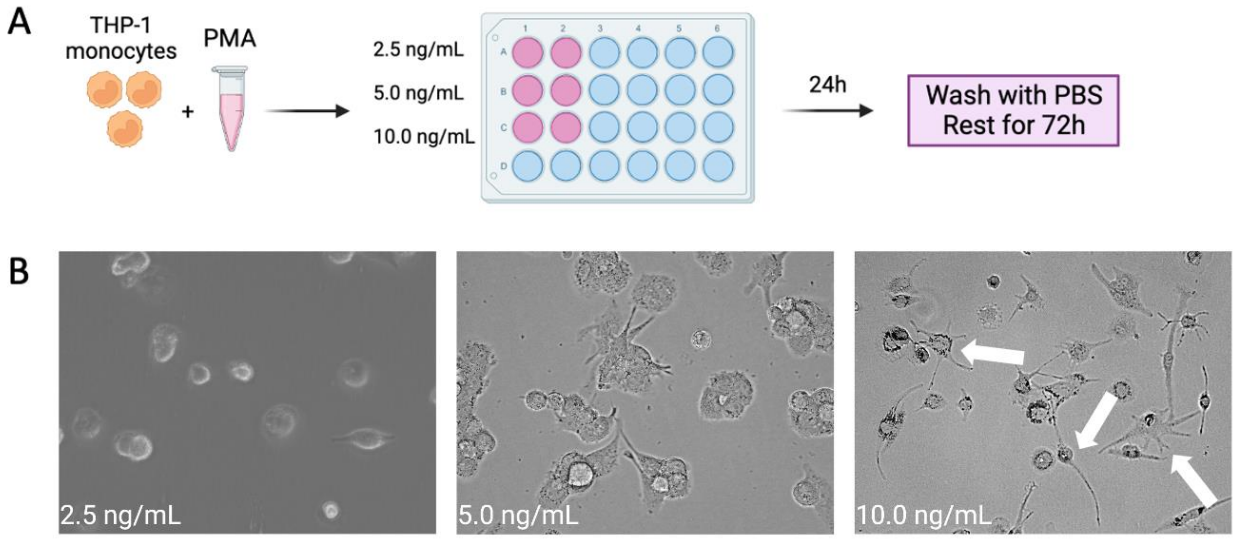

Figure 4. Differentiation of THP-1 monocytes. (A) Monocytes were induced with various concentrations of PMA for 24 hours then washed with PBS and rested for an additional 72 hours. (B) Images represent morphology of PMA-induced THP-1 macrophages at various concentrations and are indicated by the white arrow.

4.1.2 THP-1 Monocytes Require VSV-G-Env for HIV-1 infection

Although HIV-1 infection in target cells such as $CD4^+$ T cells does not require assistance of pseudotype receptor binding proteins, such as VSV-G-Env, some cell types, such as THP-1 monocytes, require the additional assistance due to their lack of specific co-receptors.

THP-1 monocytes constitutively expressing mCherry were used to determine viral infectivity. VSV-G-Env was pseudotyped with both pNL(YU-2)EGFP and pNL(BaL)iRFP proviral constructs. pNL(BaL)iRFP was a gift from the Dr. Zandrea Ambrose lab that was isolated from a lung lavage sample from a person infected with HIV-1 (Fig. 5A). pNL(YU-2)EGFP was previously constructed in our lab by cloning the *env*-containing region from the neurotropic YU-2 isolate onto the NL4-3-EGFP-IRES-X4-tropic laboratory strain via restriction sites EcoRI and

BamHI (Fig. 5B) (87). Infection of pNL(YU-2)EGFP (Fig. 6A-C) and pNL(BaL)iRFP (Fig. 6G-I) both without VSV-G-Env resulted in no replication of HIV-1 in THP-1 monocytes. However, VSV-G-Env complemented with pNL(YU-2)EGFP (Fig. 6D-F) and pNL(BaL)iRFP (Fig. 6J-L) resulted in the production and replication of HIV-1 within THP-1 monocytes, confirmed via fluorescence microscopy (Figure 6F, 6L white arrows).

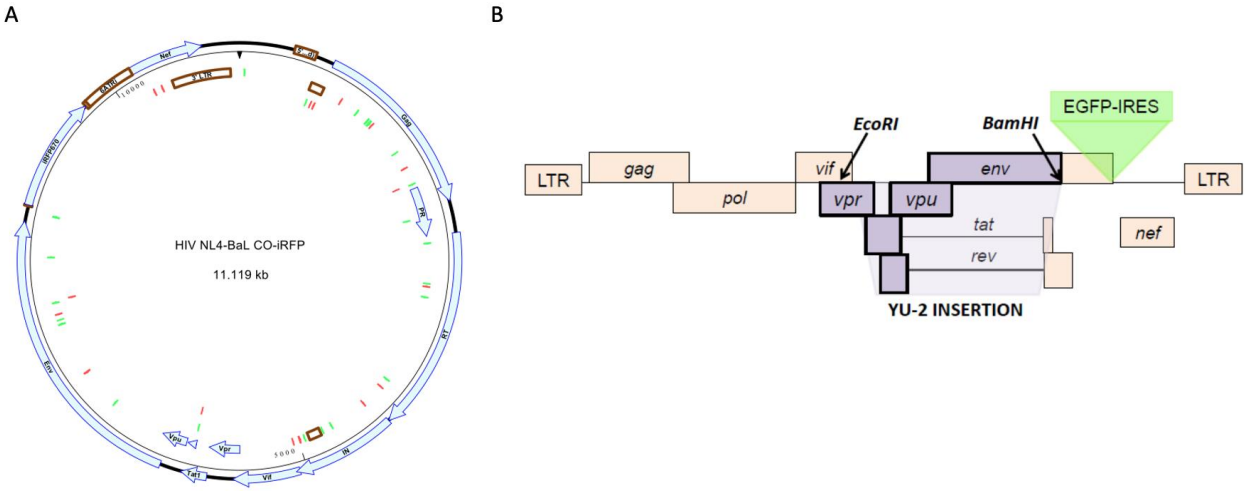

Figure 5. HIV-1 reporter viruses. (A) Genome of pNL(BaL)iRFP was a gift from the Zandrea Ambrose Laboratory. pNL(BaL)iRFP was constructed via insertion of the env-containing region of the CCR5 tropic BaL isolate onto the NL4-3-EGFP-IRES X4-tropic laboratory strain. (B) Construct of pNL(YU-2)EGFP constructed via insertion of the env-containing region of the neurotropic YU-2 isolate onto the NL4-3-EGFP-IRES X4-tropic laboratory strain.

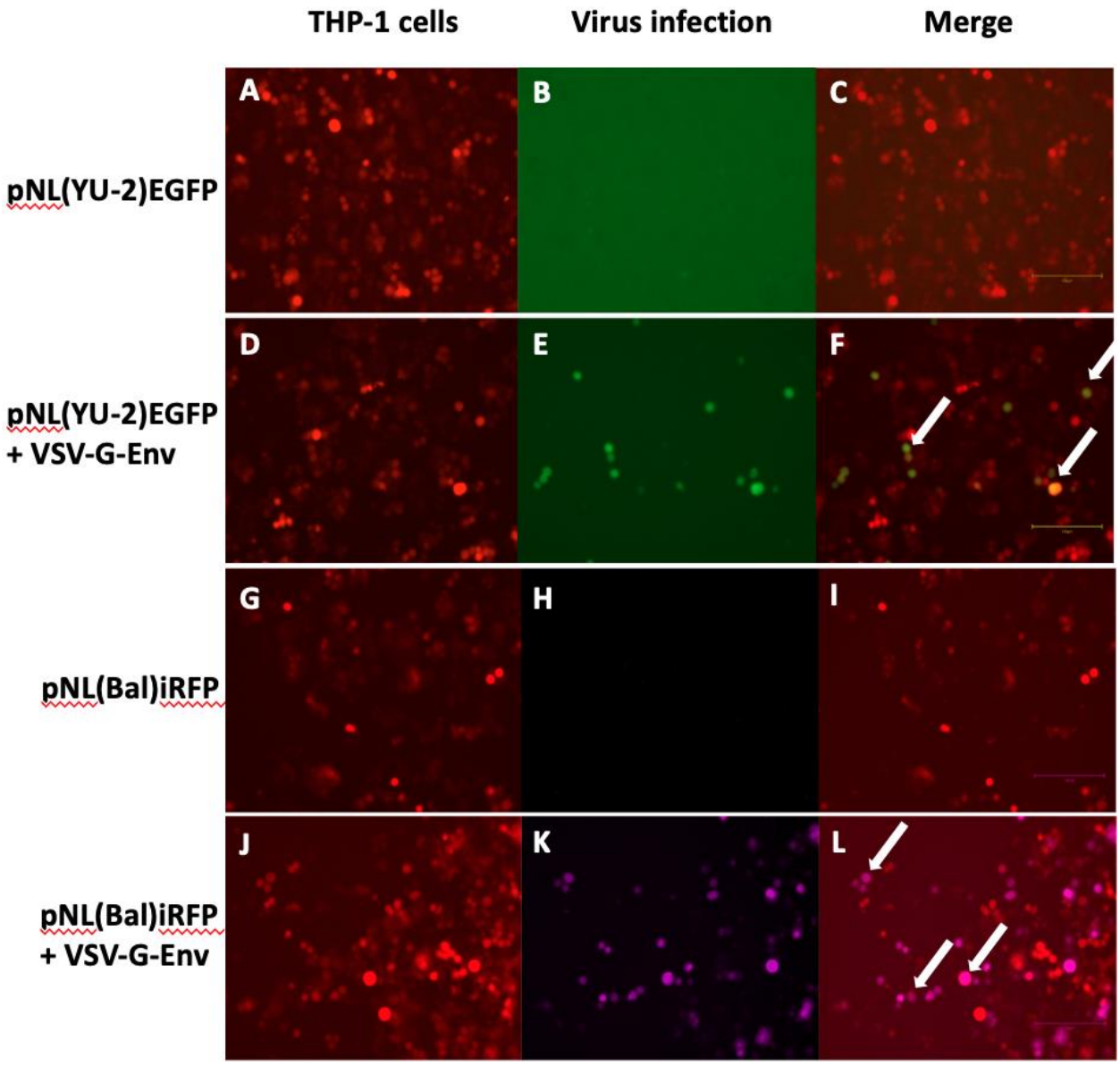

Figure 6. Infection of THP-1 monocytes with HIV-1 pseudovirus. mCherry-expressing THP-1 monocytes were infected with pNL(YU-2)EGFP without VSV-G-Env (A-C) and with VSV-G-Env (D-F), and infected with pNL(BaL)iRFP without VSV-G-Env (G-I) and with VSV-G-Enc (J-L). Infected cells are indicated by the white arrows. Images evaluated via fluorescence microscopy.

4.1.3 Assessment of Viral Kinetics in THP-1 Monocytes and PMA-Induced THP-1 Macrophages

4.1.3.1 Infection of PMA-Induced THP-1 Macrophages

To assess the various viral effects on monocytes and macrophages, THP-1 monocytes were infected, differentiated, and their morphology observed every other day for 7 days (Fig. 7). At day 7, the spindle fibers are more pronounced, exhibiting stellate morphology associated with monocyte differentiation into macrophages, as indicated by the white arrows.

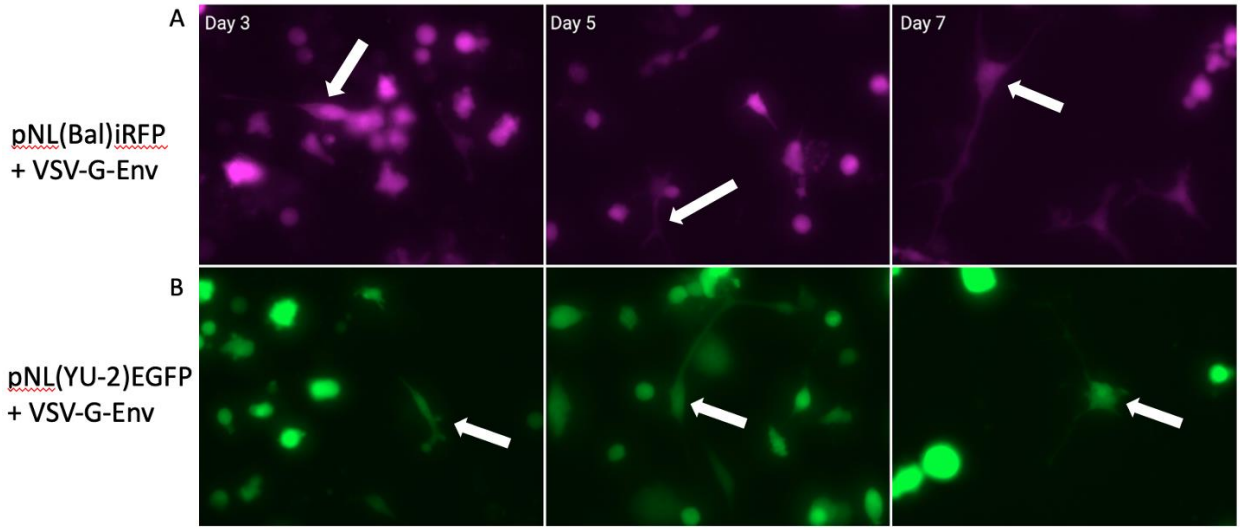

Figure 7. Infection of PMA-induced THP-1 macrophages. pNL(BaL)iRFP + VSV-G-Env (A) and pNL(YU-2)EGFP + VSV-G-Env (B) infected THP-1 monocytes were diferentiated via PMA. Images show stages of differentiation at days 3, 5, and 7. Images evaluated via fluorescence microscopy.

4.1.3.2 p24 Viral Protein Quantification

Infection of THP-1 monocytes and PMA-induced THP-1 macrophages was further confirmed through p24 ELISA analysis. THP-1 monocytes were infected with pNL(YU-2)EGFP

+ VSV-G-Env and pNL(BaL)iRFP + VSV-G-Env. After 48 hours, half of the cells were differentiated with PMA and maintained for nine days. Supernatants were collected every other day for nine days and p24 antigen was measured via ELISA. Over the course of 9 days, p24 concentration steadily increased in infected PMA-induced THP-1 macrophages (Fig. 8A-B, pink circles). THP-1 monocytes infected with pNL(YU-2)EGFP + VSV-G-Env resulted in a peak concentration of p24 at day 5 (Fig. 8A) and pNL(BaL)iRFP + VSV-G-Env continued to produce p24 protein (Fig. 8B), indicating pNL(BaL)iRFP exhibits a robust infection.

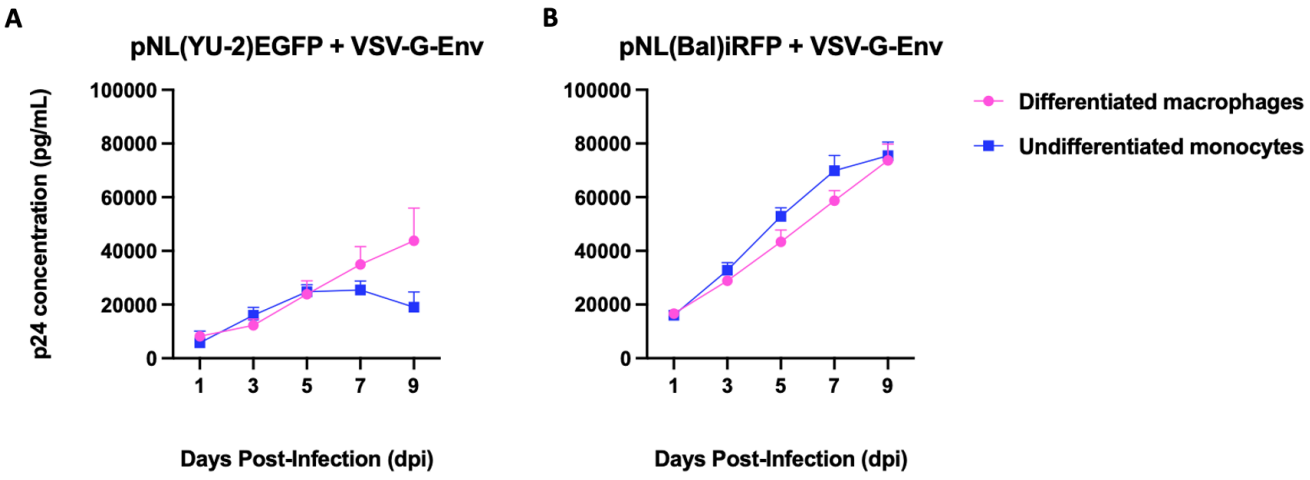

Figure 8. Quantification of viral replication in THP-1 monocytes and PMA-induced THP-1 macrophages. Cells were infected with pNL(YU-2)EGFP + VSV-G-Env (A) and pNL(BaL)iRFP + VSV-G-Env (B) and supernatant was collected every other day for p24 ELISA analysis (N=3).

4.1.3.3 Gag expression quantification

To further confirm the infectivity, infected THP-1 monocytes and PMA-induced THP-1 macrophages were collected on day 9 and analyzed for gag RNA as marker of HIV-1 infection. RNA was extracted and used to generate cDNA for RT-qPCR analysis. Fold change was measured using the comparative ΔΔCt method, and normalized to an endogenous control, glyceraldehyde 3-

phosphate dehydrogenase (GAPDH). The results show that both infections of pNL(YU-2)EGFP + VSV-G-Env and pNL(BaL)iRFP + VSV-G-Env, induced a higher expression of gag in undifferentiated monocytes than in macrophages (Fig. 9), surprisingly contradicting the previous experiment showing macrophages replicate HIV-1 at a level higher than infected THP-1 monocytes.

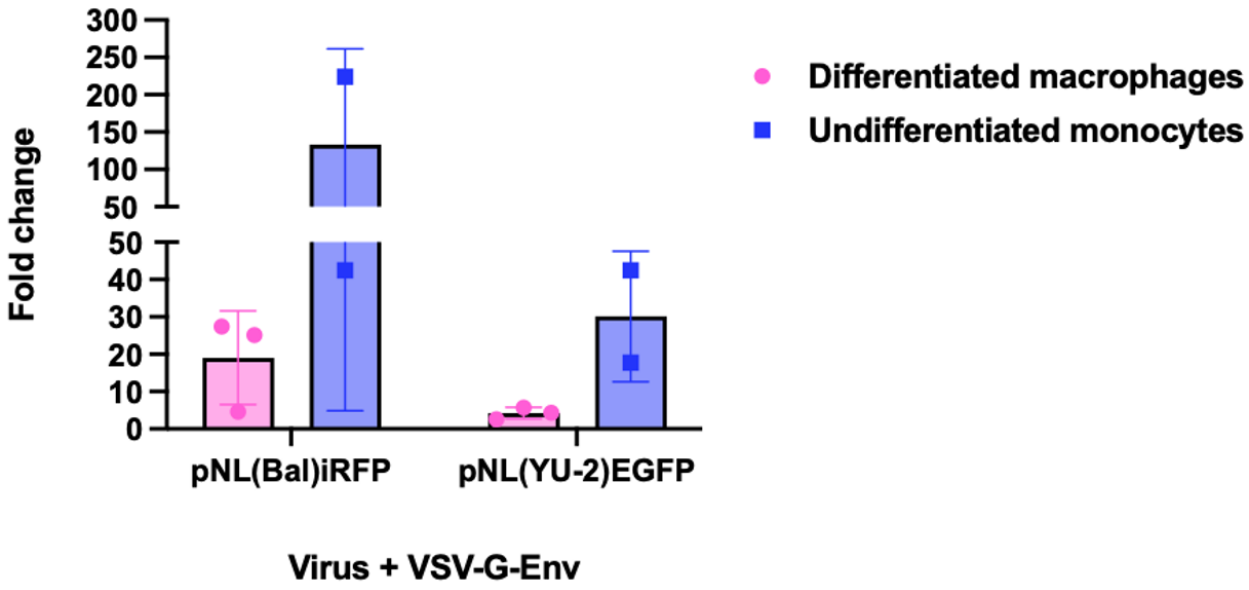

Figure 9. Expression of *gag* in THP-1 monocytes and PMA-induced macrophages. Gag expression in both infections was markedly low in macrophages (N=3, pink circles) compared to monocytes (N=2, blue squares).

4.1.3.4 Cytokine expression in response to Lipopolysaccharide (LPS)

Viral infection is known to induce inflammatory cytokine expression; therefore, we tested the expression of TNFα and IL-1β on infected and uninfected THP-1 monocytes via LPS activation. At 9 days post infection, supernatant was collected before the addition of culture media supplemented with 1 ng/mL of LPS. 16 hours later, the supernatant was collected again, and each was analyzed for TNFα and IL-1β expression via cytokine ELISA. In each case, there was a

significant increase in TNFα expression in both pNL(YU-2)EGFP + VSV-G-Env (*p<0.01*) and pNL(BaL)iRFP + VSV-G-Env (*p<0.001*) (Fig. 10) infected cultures, as expected from previous literature (88). Interestingly, pNL(BaL)iRFP + VSV-G-Env induced a stronger expression of TNFα, compared to uninfected control.

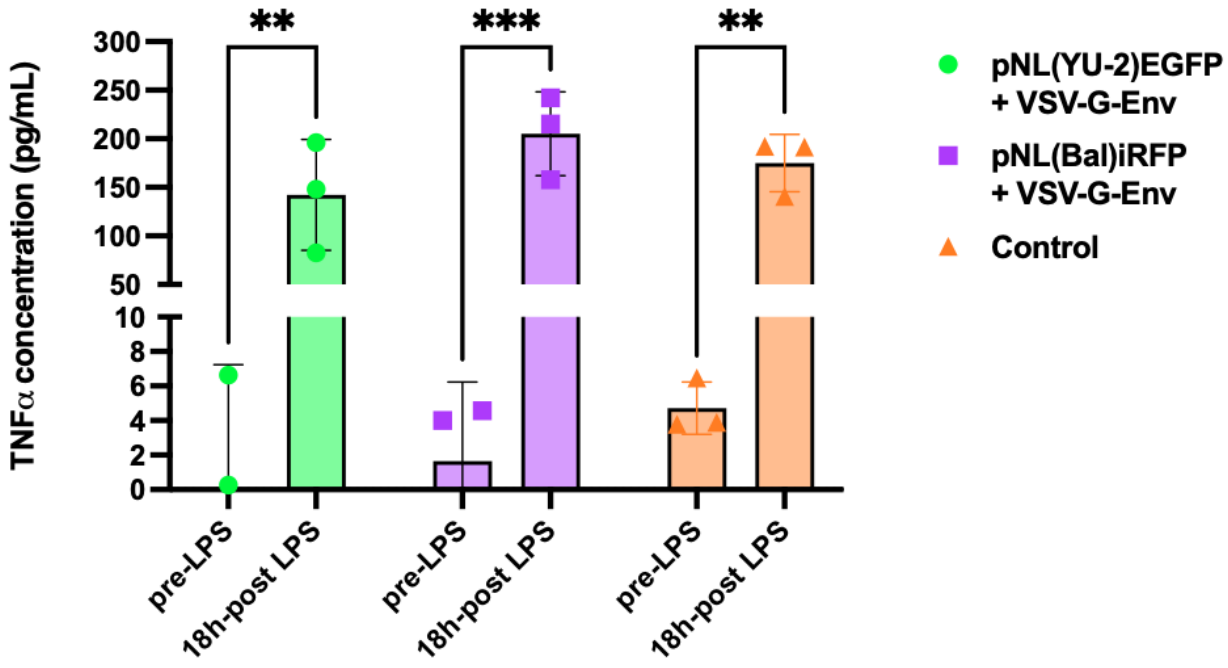

Figure 10. TNFα expression in response to LPS. Expression of TNFα was analyzed via cytokine ELISA and measured from supernatants collected 9 d.p.i. before LPS delivery, and 18 hours-post delivery. Statistical significance was determined by 2way ANOVA (*p=0.05*).

The results of the IL-1β ELISA showed the opposite, with infected THP-1 monocytes expressing a lower amount of IL-1β (Fig. 11). However, when compared to/ the concentration of the two cytokines between experiments, we can see there is a much higher production of IL-1β than TNFα before LPS delivery.

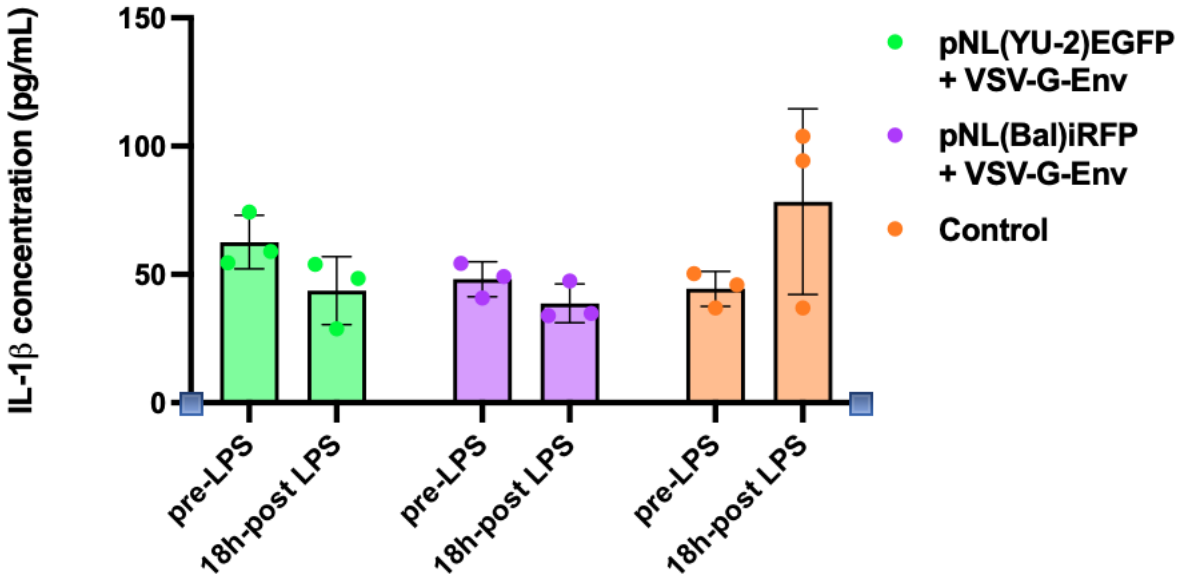

Figure 11. IL-1β expression in response to LPS. Expression of IL-1β was analyzed via cytokine ELISA and measured from supernantants collected 9 d.p.i. before LPS delivery, and 18 hours-post delivery (N=3).

4.1.4 Differentiation of $CD14^+$ Monocytes to Macrophages

Although THP-1 monocytes are the most common model to estimate modulation of monocyte and macrophage activity (89), I repeated the analysis using human primary $CD14^+$ monocytes as a physiologically relevant model. $CD14^+$ monocytes were isolated from frozen stocks of PBMCs from an HIV-negative donor via CD14 isolation and MACS column separation. For six days, cells were supplemented with GM-CSF and M-CSF, replenishing media every three days, until stellate morphology was observed (Fig. 12).

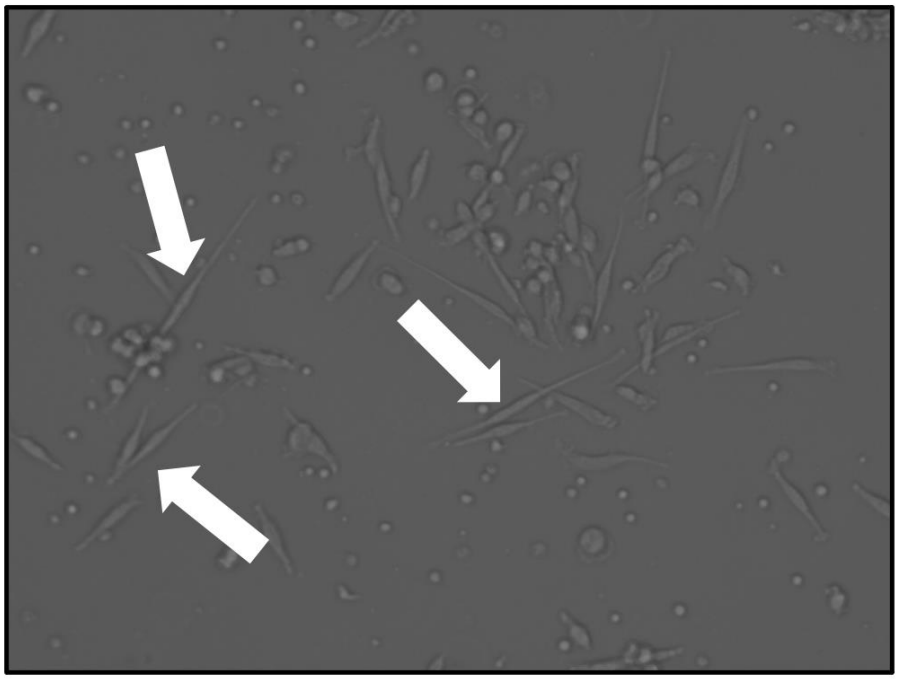

Figure 12. Differentiation of human primary $CD14^+$ monocytes. Media supplemented with GM-CSF and M-CSF were cultured with $CD14^+$ monocytes isolated from a frozen vial of PBMCs. Images taken with EVOS M5000.

4.2 Aim 2: Understand the Transmigration of Infected Monocytes and Macrophages Across the BBB *in vitro*

4.2.1 Infected THP-1 Monocytes Cross the BBB *in vitro*

In order to understand how HIV-1-infected monocytes cross the BBB and establish themselves as perivascular macrophages in the CNS, we set up a transmigration model using THP-1 cells and an 8.0 μm Transwell® inserted into the well of a tissue culture plate. Brain endothelial cells (hCMEC/D3) were seeded in the Transwell® overnight and HIV-1-infected THP-1 monocytes added to each Transwell® the following day (Fig. 13). Each Transwell® received

200,000 cells mixed with infected and uninfected THP-1 monocytes. After 48 hours, the Transwell® was removed and cells were observed at the bottom of the well, with the hCMEC/D3 cells still seeded in the Transwell® . Cells that migrated to the bottom well were counted and the amount of infected and uninfected cells were graphed (Fig. 14). Infected cells were confirmed via fluorescence microscopy. In both infections and the control, the same number of THP-1 monocytes migrated across the Transwell®, with uninfected cells migrating at a much higher rate than infected monocytes.

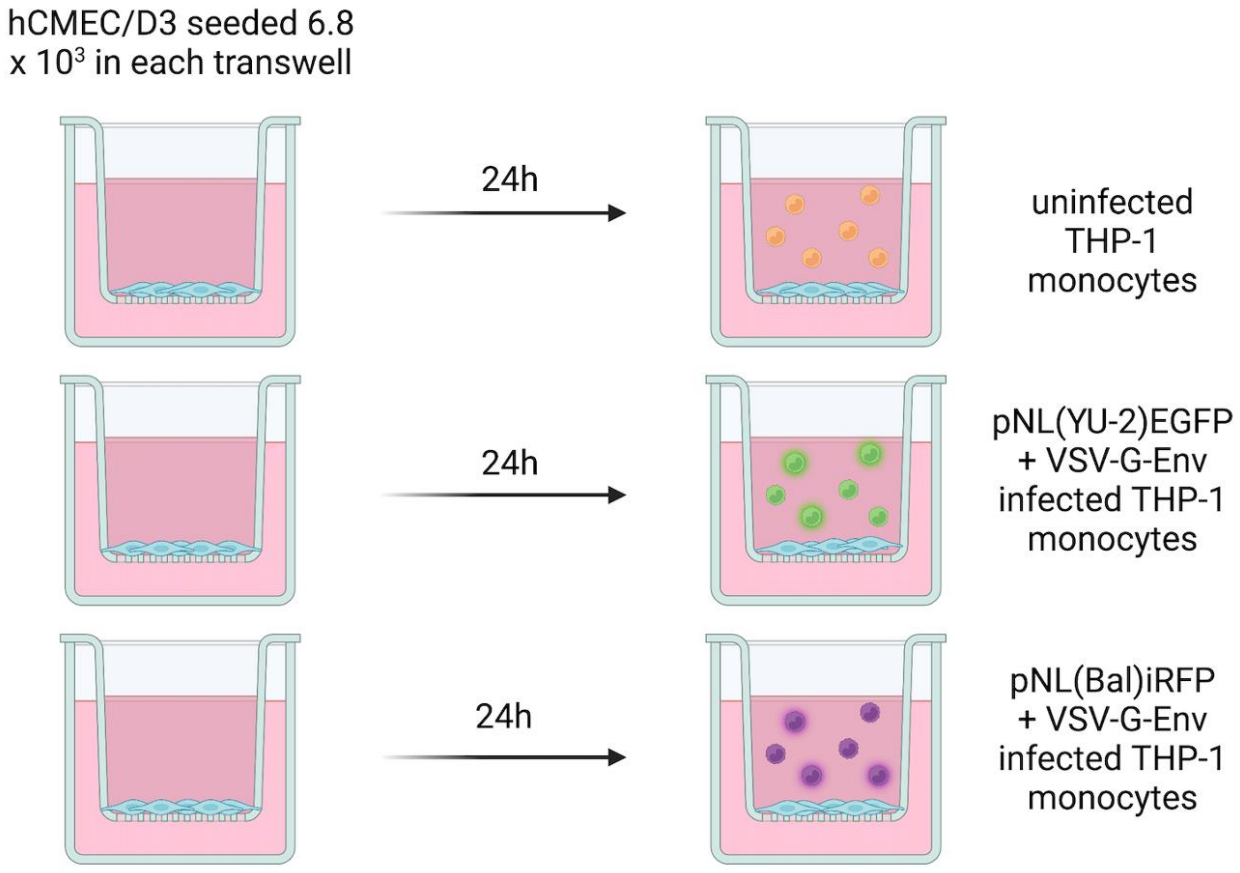

Figure 13. Experimental design of infected THP-1 monocyte migration across the BBB. hCMEC/D3 brain endothelial cells were seeded in a Transwell® for 24 hours before the addition of infected THP-1 monocytes.

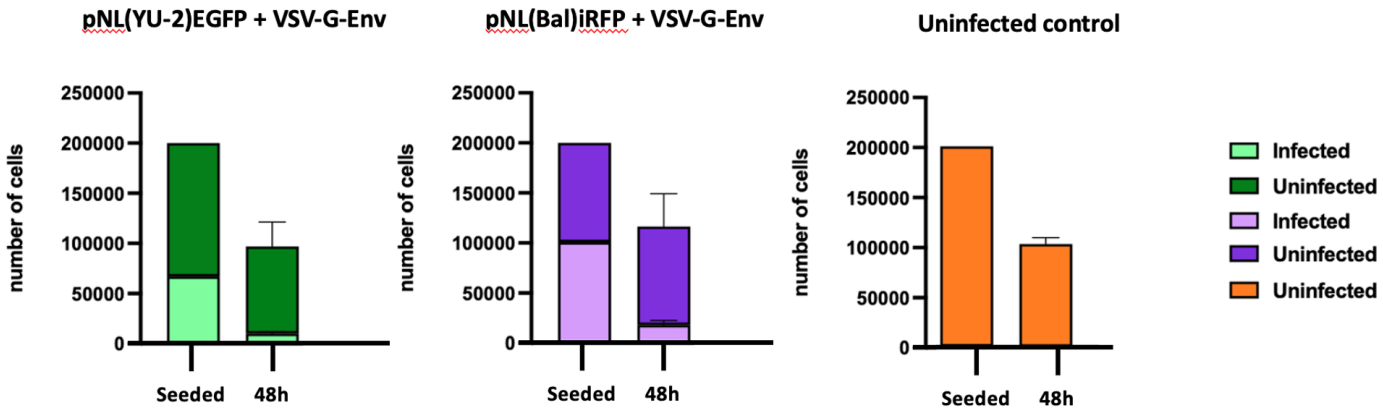

Figure 14. Number of THP-1 monocytes across the BBB. 200,000 THP-1-infected monocytes were added to a Transwell® set up. The cells that migrated across the Transwell® were counted 48 hours later (N=3).

5.0 Conclusions and Discussion

The progression of HIV-1 associated neurocognitive diseases is caused by HIV-1-infected monocytes transmigrating across the blood-brain barrier and establishing themselves as perivascular macrophages in the central nervous system (74, 75). However, our understanding of how infected monocytes from the periphery transmigrate into the CNS is limited due to the lack of a relevant *in vitro* blood-brain barrier model. The aims of my thesis are to improve the established *in vitro* 3D-brain organoid model by incorporating brain endothelial cells to mimic the blood-brain barrier. To accomplish this, I proposed the following aims: characterize the mechanics of monocyte and macrophage infection *in vitro* and understand how infected monocytes transmigrate across the BBB *in vitro*.

It is well established that HIV-1-infected macrophages become viral reservoirs capable of harboring viral DNA and producing low levels of viral protein to further the course of disease development. Within the CNS, the accumulation of these HIV-1-infected macrophages contributes to the neurological dysfunctions associated with HAND (20, 71, 80, 90). Therefore, I decided to test HIV-1 infection in both monocytes and macrophages to understand how each cell type responds to viral infection *in vitro*. To differentiate monocytes to macrophages, THP-1 monocytes were maintained in media supplemented with PMA, a mitogen that induces macrophage differentiation (85, 91). Three concentrations were chosen to test optimal differentiation of monocytes, 2.5 ng/mL, 5.0 ng/mL, and 10.0 ng/mL. After 72 hours, 5 ng/mL of PMA was able to induce adherent cells but was not enough to produce spindle-like fibers associated with macrophage morphology, and 2.5 ng/mL was not sufficient at all and resulted in non-adherent cells (Fig. 4B). A concentration of 10 ng/mL was capable of inducing adherent cells that exhibited

spindle-like fibers and stellate morphology of macrophages (Fig. 4), confirming the protocol by Baxter et al. and Smith et al. (85, 86).

To study cellular immune responses in an *in vitro* model, THP-1 monocytic cells were used to standardize HIV-1 infection in cells capable of transmigrating across an *in vitro* BBB (89, 92). THP-1 cells are widely used to study both monocytes and macrophages as an alternative to primary human blood samples, due to the ease of access, long term storage, and high rate of replication (93). Before investigating transmigration, infection with HIV-reporter viruses was optimized using a VSV-G-Env pseudotyped virus. Studies have shown, pseudotyping VSV-G-Env with HIV-1 isolates enables viral entry via endocytosis, circumventing CCR5 and CD4 co-receptors, as well as activating a robust infection, giving the virus a 20- to 130-fold higher infectivity (94–96). THP-1 monocytes express very low levels of CD4 and CCR5, furthering the need to use VSV-G-Env pseudotyped virus in HIV-1 infection (97). THP-1 monocytes stably transduced with mCherry were used to determine cellular morphology and infection state with VSV-G-Env pseudotyped HIV-1 virus, resulted in HIV-1 viral entry and replication confirmed via fluorescent signal (Fig. 6F, 6L). Infecting THP-1 monocytes with pseudotyped HIV-1 virus lacking VSV-G-Env did not result in infection, as the virus was unable to enter the cells (Fig. 6C, 6I). In addition, we differentiated pseudotyped infected THP-1 monocytes with 10 ng/mL of PMA and again observed viral replication within PMA-induced THP-1 macrophages via fluorescent signal (Fig. 7). Having confirmed that our pseudotyped virus could enter both THP-1 monocytes and PMA-induced macrophages, I next determined the viral replication kinetics to assess whether they exhibit any differences *in vitro*.

To further confirm the visualization of viral replication within THP-1 monocytes and PMA-induced THP-1 macrophages, viral quantification was assessed via ELISA and RT-qPCR

analyses. The capsid protein of HIV-1, known as p24 viral antigen, is the most abundant viral protein and is present at high levels throughout all stages of HIV-1 infection (in the absence of ART) (98). PMA-induced THP-1 macrophages infected with HIV-1-reporter viruses, exhibited a steady increase in p24 viral replication (Fig. 8), an expected outcome since macrophages permit HIV-1 entry, support viral replication, and are relatively less prone to the cytopathic effects of HIV-1 (99, 100). The results obtained with the undifferentiated monocytes remain inconclusive. THP-1 monocytes infected with pNL(BaL)iRFP + VSV-G-Env resulted in robust viral replication, but pNL(YU-2)EGFP + VSV-G-Env infected monocytes produce less virus over time. It could be due to the fact that one virus has a higher level of infectivity than the other, and if time were extended, we could possibly see the downward slope of the replication peak seen in Fig. 8B.

In addition to quantifying viral replication via p24 ELISA, I further confirmed viral replication by quantifying the expression of viral proteins, specifically *gag* gene expression. Gag is a major structural protein whose main functions include capsid formation, viral assembly, and intracellular trafficking (101, 102). More specifically, the gag gene encodes a precursor protein that is cleaved by protease into multiple different proteins, including p24 (103). Quantifying gag gene expression via RT-qPCR contradicted the decrease in p24 expression in monocytes, suggesting monocytes express gag at a higher fold change than differentiated macrophages (Fig. 9). Due to time constraints, only one independent experiment was run, and when purifying the RNA from uninfected THP-1 monocytes, the concentration was insufficient to produce complete cDNA, needed to normalize the RT-qPCR data. In addition, one of the infected THP-1 monocyte samples had a triplicate sample that was half the Ct value as the other two replicates, possibly contributing to the vast range seen in pNL(BaL)iRFP undifferentiated monocytes (Fig. 9).

Additional replicative experiments are needed to conclusively determine the differential *gag* expression and p24 released in the supernatant between monocytes and macrophages.

HIV-1-infected monocytes and macrophages secrete pro-inflammatory cytokines, specifically tumor necrosis factor-α (TNFα) and interleukin-1β (IL-1β), which can induce cytotoxic effects, such as neuronal death and decreased BBB integrity, subsequently allowing HIV-1-infected monocytes into the CNS (104–106). In my studies, THP-1 monocytes were infected with both our pseudotyped HIV-1 reporter viruses with supernatant collected 9 d.p.i. LPS was added to the culture to induce pro-inflammatory cytokines and their concentrations were compared between pre- and post-LPS activation. LPS was used to determine the maximum amount of pro-inflammatory secretion these cells were capable of. Results from my study indicated that TNFα expression was significantly increased upon LPS activation (Fig. 10). More importantly, even in the absence of TNFα production (Fig. 10, pNL(YU-2)EGFP + VSV-G-Env) replicates 1 & 2 exhibited a robust expression of TNFα, comparable to that of the control, and these results are in accordance with previous findings (107). Conversely, the expression of IL-1β decreased in response to LPS (Fig. 11) compared to the response from TNFα. Albeit the levels of IL-1β expression were higher pre-LPS exposure compared to TNFα. These results conclude that pro-inflammatory cytokines can be measured pre- and post-LPS exposure, observing differences in the expression of TNFα and IL-1β. It is also possible to predict that expression of cytokines may vary as they may not express at the same time point post-LPS stimulation.

Altogether, I was able to infect THP-1 monocytes with a VSV-G-Env pseudotyped virus resulting in a robust infection that was quantifiable in both p24 ELISA and RT-qPCR of *gag* gene expression analyses, resulting in cell types that mimic the effects associated with HIV-1-infection in monocytes and macrophages. Having established a cell line-based protocol for HIV-1 infection,

I next sought to investigate migration of infected and uninfected THP-1 monocytes and PMA-induced THP-1 macrophages across the BBB model. My second aim involves understanding the migration of THP-1 monocytes and macrophages across our brain endothelial barrier. To begin investigating transmigration of HIV-1-infected THP-1 monocytes, brain endothelial cells were seeded into the Transwell® set-up described above (Fig.13). At 48 hours, post-introduction of THP-1s, a majority of the uninfected monocytes crossed the Transwell®, with a few infected monocytes crossing over as well (Fig. 14). This may be due to an insufficient number of hCMEC/D3 cells in the Transwell® resulting in an incomplete barrier. The size of the Transwell® may be too large, allowing these cells to pass through the barrier within 48 hours. Next steps will include troubleshooting and optimizing the model to ensure a complete barrier and appropriately sized wells to confirm these results. Once the hCMEC/D3 brain endothelial barrier is optimized, human primary monocytes can be added to the model and various viral kinetics analyzed and observed.

The isolation and differentiation of human primary $CD14^+$ monocytes to macrophages (Fig. 12) are an essential part of the BBB model. There are limitations in using the THP-1 cell line, including a decreased response to LPS compared to human primary monocytes, since they have low expression of CD14 cell surface markers (108). It is also important to note, using human primary cells over immortalized cell lines, produces more translatable results to the application of real-world physiology. $CD14^+$ monocytes express HIV-1 co-receptors, permitting the entry of HIV-1 without the use of a pseudotyped virus. However, due to the lack of access to healthy blood donors, only one round of differentiation was performed, which was consumed by infection on day 2. Two frozen vials of PBMCs were used to isolate $CD14^+$ monocytes, but due to complications with freezing, the cell did not differentiate into macrophages.

After the brain endothelial cell barrier is optimized, and fresh $CD14^+$ monocytes obtained for viral kinetics, the transmigration of infected and uninfected monocytes/macrophages can be fully observed and the effects of analyzed. Additionally, more cell types can be incorporated into the model, including brain organoids and astrocytes, that could significantly impact the understanding of the BBB, in hopes of identifying a novel therapeutic that targets HIV-1 in the CNS.

6.0 Future Directions

Incorporating brain endothelial cells (hCMEC/D3) into the 3D-brain organoid model is another step toward the development of a physiologically relevant model to study HIV-1 in the central nervous system. Using the Transwell® set up, continued analyses is needed to determine the migration of infected monocytes across the BBB, including the optimization of endothelial resistance in hCMEC/D3 cells.

To further increase biological relevance, human primary $CD14^+$ monocytes must be obtained and analyzed for viral replication kinetics, such as p24 production, *gag* expression, cytokine ELISA induction, and differentiation to macrophages to better mimic the physiological characteristics of human monocytes in the CNS. Altogether, the incorporation of the BBB and human primary monocytes, along with the addition of other cell types such as astrocytes and microglia, will help conduct studies to investigate potential therapeutics that penetrate the BBB and target infected cells.

7.0 Public Health Significance

HIV-1 has been a crucial public health concern since it was first identified in the 1980's. Although HIV-1infection primarily affects the immune system, it can also cause other comorbidities including neurological complications. One of the critical factors that contribute to HIV-associated neurological diseases is the ability of infected monocytes to cross the blood-brain barrier from the periphery into the central nervous system, differentiate into perivascular macrophages and establishes infection in the CNS (29, 31, 68–70). In order to study the transmigration of HIV-1-infected monocytes across the BBB, a physiologically relevant model is needed to understand the mechanisms that drive the symptoms of HAND. In addition, cART drugs have been successful in suppressing virus in the periphery but are unable to penetrate the CNS and suppress viral load in the brain (18, 19)**.**

Previously, our lab developed a 3D-brain organoid model used to study the neuropathogenesis of HIV-1 infection in the central nervous system. By incorporating brain endothelial cells to the model, the interaction between monocytes and the BBB can help researchers identify potential therapeutic targets to prevent HIV-1-related brain damage, as well as develop new diagnostic tools for early detection of neurological complications in PLWH (109). As such, the scope of this research contributes to the field of public health.

Bibliography

1. Sepkowitz KA. 2001. AIDS — The First 20 Years. N Engl J Med 344:1764–1772.

2. WHO. 2022. HIV.

3. Sharp PM, Hahn BH. 2011. Origins of HIV and the AIDS Pandemic. Cold Spring Harbor Perspectives in Medicine 1:a006841–a006841.

4. Deeks SG, Overbaugh J, Phillips A, Buchbinder S. 2015. HIV infection. Nat Rev Dis Primers 1:15035.

5. Galvin SR, Cohen MS. 2004. The role of sexually transmitted diseases in HIV transmission. Nat Rev Microbiol 2:33–42.

6. Shaw GM, Hunter E. 2012. HIV Transmission. Cold Spring Harbor Perspectives in Medicine 2:a006965–a006965.

7. Hu W-S, Hughes SH. 2012. HIV-1 Reverse Transcription. Cold Spring Harbor Perspectives in Medicine 2:a006882–a006882.

8. Craigie R, Bushman FD. 2012. HIV DNA Integration. Cold Spring Harbor Perspectives in Medicine 2:a006890–a006890.

9. Balasubramaniam M, Pandhare J, Dash C. 2019. Immune Control of HIV. J Life Sci (Westlake Village) 1:4–37.

10. Giorgi JV, Lyles RH, Matud JL, Yamashita TE, Mellors JW, Hultin LE, Jamieson BD, Margolick JB, Rinaldo Jr CR, Phair JP, Detels R. 2002. Predictive Value of Immunologic and Virologic Markers After Long or Short Duration of HIV-1 Infection: JAIDS Journal of Acquired Immune Deficiency Syndromes 29:346–355.

11. Deeks SG, Kitchen CMR, Liu L, Guo H, Gascon R, Narváez AB, Hunt P, Martin JN, Kahn JO, Levy J, McGrath MS, Hecht FM. 2004. Immune activation set point during early HIV infection predicts subsequent CD4+ T-cell changes independent of viral load. Blood 104:942–947.

12. Schüpbach J. 2002. Measurement of HIV-1 p24 antigen by signal-amplification-boosted ELISA of heat-denatured plasma is a simple and inexpensive alternative to tests for viral RNA. AIDS Rev 4:83–92.

13. Anderson AM, Tyor WR, Mulligan MJ, Waldrop-Valverde D, Lennox JL, Letendre SL. 2018. Measurement of Human Immunodeficiency Virus p24 Antigen in Human Cerebrospinal Fluid With Digital Enzyme-Linked Immunosorbent Assay and Association With Decreased Neuropsychological Performance. Clinical Infectious Diseases 67:137–140.

14. Simon V, Ho DD, Abdool Karim Q. 2006. HIV/AIDS epidemiology, pathogenesis, prevention, and treatment. The Lancet 368:489–504.

15. Arts EJ, Hazuda DJ. 2012. HIV-1 Antiretroviral Drug Therapy. Cold Spring Harbor Perspectives in Medicine 2:a007161–a007161.

16. Menéndez-Arias L, Delgado R. 2022. Update and latest advances in antiretroviral therapy. Trends in Pharmacological Sciences 43:16–29.

17. 2021. Is "Undetectable = Untransmissible" Good Public Health Messaging? AMA Journal of Ethics 23:E418-422.

18. Eggers C, Arendt G, Hahn K, Husstedt IW, Maschke M, Neuen-Jacob E, Obermann M, Rosenkranz T, Schielke E, Straube E. 2017. HIV-1-associated neurocognitive disorder: epidemiology, pathogenesis, diagnosis, and treatment. J Neurol 264:1715–1727.

19. Machado Andrade V, Stevenson M. 2019. Host and Viral Factors Influencing Interplay between the Macrophage and HIV-1. J Neuroimmune Pharmacol 14:33–43.

20. Saylor D, Dickens AM, Sacktor N, Haughey N, Slusher B, Pletnikov M, Mankowski JL, Brown A, Volsky DJ, McArthur JC. 2016. HIV-associated neurocognitive disorder — pathogenesis and prospects for treatment. Nat Rev Neurol 12:234–248.

21. Sacktor N, Skolasky RL, Seaberg E, Munro C, Becker JT, Martin E, Ragin A, Levine A, Miller E. 2016. Prevalence of HIV-associated neurocognitive disorders in the Multicenter AIDS Cohort Study. Neurology 86:334–340.

22. Heaton RK, Franklin DR, Ellis RJ, McCutchan JA, Letendre SL, LeBlanc S, Corkran SH, Duarte NA, Clifford DB, Woods SP, Collier AC, Marra CM, Morgello S, Mindt MR, Taylor MJ, Marcotte TD, Atkinson JH, Wolfson T, Gelman BB, McArthur JC, Simpson DM, Abramson I, Gamst A, Fennema-Notestine C, Jernigan TL, Wong J, Grant I. 2011. HIV-associated neurocognitive disorders before and during the era of combination antiretroviral therapy: differences in rates, nature, and predictors. J Neurovirol 17:3–16.

23. Ellis RJ, Calero P, Stockin MD. 2009. HIV Infection and the Central Nervous System: A Primer. Neuropsychol Rev 19:144–151.

24. Wahl A, Al-Harthi L. 2023. HIV infection of non-classical cells in the brain. Retrovirology 20:1.

25. Sacktor N. 2018. Changing clinical phenotypes of HIV-associated neurocognitive disorders. J Neurovirol 24:141–145.

26. Nightingale S, Winston A, Letendre S, Michael BD, McArthur JC, Khoo S, Solomon T. 2014. Controversies in HIV-associated neurocognitive disorders. The Lancet Neurology 13:1139–1151.

27. Rosenthal J, Tyor W. 2019. Aging, comorbidities, and the importance of finding biomarkers for HIV-associated neurocognitive disorders. J Neurovirol 25:673–685.

28. Valcour V, Chalermchai T, Sailasuta N, Marovich M, Lerdlum S, Suttichom D, Suwanwela NC, Jagodzinski L, Michael N, Spudich S, Van Griensven F, De Souza M, Kim J, Ananworanich J. 2012. Central Nervous System Viral Invasion and Inflammation During Acute HIV Infection. The Journal of Infectious Diseases 206:275–282.

29. Spudich S, Gonzalez-Scarano F. 2012. HIV-1-Related Central Nervous System Disease: Current Issues in Pathogenesis, Diagnosis, and Treatment. Cold Spring Harbor Perspectives in Medicine 2:a007120–a007120.

30. González-Scarano F, Martín-García J. 2005. The neuropathogenesis of AIDS. Nat Rev Immunol 5:69–81.

31. Ene L. 2018. Human Immunodeficiency Virus in the Brain—Culprit or Facilitator? Infect Dis (Auckl) 11:117863371775268.

32. De Luca A, Ciancio BC, Larussa D, Murri R, Cingolani A, Rizzo MG, Giancola ML, Ammassari A, Ortona L. 2002. Correlates of independent HIV-1 replication in the CNS and of its control by antiretrovirals. Neurology 59:342–347.

33. Atluri VSR, Hidalgo M, Samikkannu T, Kurapati KRV, Jayant RD, Sagar V, Nair MPN. 2015. Effect of human immunodeficiency virus on blood-brain barrier integrity and function: an update. Front Cell Neurosci 9.

34. He Q, Liu J, Liang J, Liu X, Li W, Liu Z, Ding Z, Tuo D. 2018. Towards Improvements for Penetrating the Blood–Brain Barrier—Recent Progress from a Material and Pharmaceutical Perspective. Cells 7:24.

35. Strazza M, Pirrone V, Wigdahl B, Nonnemacher MR. 2011. Breaking down the barrier: The effects of HIV-1 on the blood–brain barrier. Brain Research 1399:96–115.

36. Ivey NS, MacLean AG, Lackner AA. 2009. Acquired immunodeficiency syndrome and the blood-brain barrier. J Neurovirol 15:111–122.

37. Morita K, Sasaki H, Furuse M, Tsukita S. 1999. Endothelial Claudin. Journal of Cell Biology 147:185–194.

38. Abbott NJ, Patabendige AAK, Dolman DEM, Yusof SR, Begley DJ. 2010. Structure and function of the blood–brain barrier. Neurobiology of Disease 37:13–25.

39. Cereijido M, Shoshani L, Contreras RG. 2000. Molecular Physiology and Pathophysiology of Tight Junctions I. Biogenesis of tight junctions and epithelial polarity. American Journal of Physiology-Gastrointestinal and Liver Physiology 279:G477–G482.

40. Ballabh P, Braun A, Nedergaard M. 2004. The blood–brain barrier: an overview. Neurobiology of Disease 16:1–13.

41. Piantino M, Louis F, Shigemoto-Mogami Y, Kitamura K, Sato K, Yamaguchi T, Kawabata K, Yamamoto S, Iwasaki S, Hirabayashi H, Matsusaki M. 2022. Brain microvascular endothelial cells derived from human induced pluripotent stem cells as in vitro model for assessing blood-brain barrier transferrin receptor-mediated transcytosis. Materials Today Bio 14:100232.

42. Langen UH, Ayloo S, Gu C. 2019. Development and Cell Biology of the Blood-Brain Barrier. Annu Rev Cell Dev Biol 35:591–613.

43. Abbott NJ, Rönnbäck L, Hansson E. 2006. Astrocyte–endothelial interactions at the blood–brain barrier. Nat Rev Neurosci 7:41–53.

44. Wong AD, Ye M, Levy AF, Rothstein JD, Bergles DE, Searson PC. 2013. The blood-brain barrier: an engineering perspective. Front Neuroeng 6.

45. Kimelberg HK, Nedergaard M. 2010. Functions of astrocytes and their potential as therapeutic targets. Neurotherapeutics 7:338–353.

46. Kubotera H, Ikeshima-Kataoka H, Hatashita Y, Allegra Mascaro AL, Pavone FS, Inoue T. 2019. Astrocytic endfeet re-cover blood vessels after removal by laser ablation. Sci Rep 9:1263.

47. Mathiisen TM, Lehre KP, Danbolt NC, Ottersen OP. 2010. The perivascular astroglial sheath provides a complete covering of the brain microvessels: An electron microscopic 3D reconstruction. Glia 58:1094–1103.

48. Yao Y, Chen Z-L, Norris EH, Strickland S. 2014. Astrocytic laminin regulates pericyte differentiation and maintains blood brain barrier integrity. Nat Commun 5:3413.

49. Szu JI, Binder DK. 2016. The Role of Astrocytic Aquaporin-4 in Synaptic Plasticity and Learning and Memory. Front Integr Neurosci 10.

50. Quaegebeur A, Segura I, Carmeliet P. 2010. Pericytes: Blood-Brain Barrier Safeguards against Neurodegeneration? Neuron 68:321–323.

51. Lai C-H, Kuo K-H. 2005. The critical component to establish in vitro BBB model: Pericyte. Brain Research Reviews 50:258–265.

52. Guillemin GJ, Brew BJ. 2004. Microglia, macrophages, perivascular macrophages, and pericytes: a review of function and identification. Journal of Leukocyte Biology 75:388–397.

53. Armulik A, Genové G, Mäe M, Nisancioglu MH, Wallgard E, Niaudet C, He L, Norlin J, Lindblom P, Strittmatter K, Johansson BR, Betsholtz C. 2010. Pericytes regulate the blood–brain barrier. Nature 468:557–561.

54. Faraco G, Park L, Anrather J, Iadecola C. 2017. Brain perivascular macrophages: characterization and functional roles in health and disease. J Mol Med 95:1143–1152.

55. Kim W-K, Alvarez X, Fisher J, Bronfin B, Westmoreland S, McLaurin J, Williams K. 2006. CD163 Identifies Perivascular Macrophages in Normal and Viral Encephalitic Brains and Potential Precursors to Perivascular Macrophages in Blood. The American Journal of Pathology 168:822–834.

56. Fabriek BO, Van Haastert ES, Galea I, Polfliet MMJ, Döpp ED, Van Den Heuvel MM, Van Den Berg TK, De Groot CJA, Van Der Valk P, Dijkstra CD. 2005. CD163-positive perivascular macrophages in the human CNS express molecules for antigen recognition and presentation. Glia 51:297–305.

57. Yang T, Guo R, Zhang F. 2019. Brain perivascular macrophages: Recent advances and implications in health and diseases. CNS Neurosci Ther 25:1318–1328.

58. Willis CL, Garwood CJ, Ray DE. 2007. A size selective vascular barrier in the rat area postrema formed by perivascular macrophages and the extracellular matrix. Neuroscience 150:498–509.

59. Li Y, Zhu Z, Huang T, Zhou Y, Wang X, Yang L, Chen Z, Yu W, Li P. 2018. The peripheral immune response after stroke—A double edge sword for blood-brain barrier integrity. CNS Neurosci Ther 24:1115–1128.

60. Graeber MB, Streit WJ. 2010. Microglia: biology and pathology. Acta Neuropathol 119:89–105.

61. Kierdorf K, Erny D, Goldmann T, Sander V, Schulz C, Perdiguero EG, Wieghofer P, Heinrich A, Riemke P, Hölscher C, Müller DN, Luckow B, Brocker T, Debowski K, Fritz G, Opdenakker G, Diefenbach A, Biber K, Heikenwalder M, Geissmann F, Rosenbauer F, Prinz M. 2013. Microglia emerge from erythromyeloid precursors via Pu.1- and Irf8-dependent pathways. Nat Neurosci 16:273–280.

62. Wolf SA, Boddeke HWGM, Kettenmann H. 2017. Microglia in Physiology and Disease. Annu Rev Physiol 79:619–643.

63. Wallet C, De Rovere M, Van Assche J, Daouad F, De Wit S, Gautier V, Mallon PWG, Marcello A, Van Lint C, Rohr O, Schwartz C. 2019. Microglial Cells: The Main HIV-1 Reservoir in the Brain. Front Cell Infect Microbiol 9:362.

64. Cenker JJ, Stultz RD, McDonald D. 2017. Brain Microglial Cells Are Highly Susceptible to HIV-1 Infection and Spread. AIDS Research and Human Retroviruses 33:1155–1165.

65. Joseph SB, Arrildt KT, Sturdevant CB, Swanstrom R. 2015. HIV-1 target cells in the CNS. J Neurovirol 21:276–289.

66. Lawson LJ, Perry VH, Gordon S. 1992. Turnover of resident microglia in the normal adult mouse brain. Neuroscience 48:405–415.

67. Gega A, Kozal MJ, Chiarella J, Lee E, Peterson J, Hecht FM, Liegler T, St John EP, Simen BB, Price RW, Spudich SS. 2015. Deep sequencing of HIV-1 variants from paired plasma

and cerebrospinal fluid during primary HIV infection. Journal of Virus Eradication 1:264–268.

68. Rojas-Celis V, Valiente-Echeverría F, Soto-Rifo R, Toro-Ascuy D. 2019. New Challenges of HIV-1 Infection: How HIV-1 Attacks and Resides in the Central Nervous System. Cells 8:1245.

69. Schnell G, Price RW, Swanstrom R, Spudich S. 2010. Compartmentalization and Clonal Amplification of HIV-1 Variants in the Cerebrospinal Fluid during Primary Infection. J Virol 84:2395–2407.

70. Ellery PJ, Tippett E, Chiu Y-L, Paukovics G, Cameron PU, Solomon A, Lewin SR, Gorry PR, Jaworowski A, Greene WC, Sonza S, Crowe SM. 2007. The CD16+ Monocyte Subset Is More Permissive to Infection and Preferentially Harbors HIV-1 In Vivo. The Journal of Immunology 178:6581–6589.

71. Wong ME, Jaworowski A, Hearps AC. 2019. The HIV Reservoir in Monocytes and Macrophages. Front Immunol 10:1435.

72. Pulliam L, Gascon R, Stubblebine M, McGuire D, McGrath MS. 1997. Unique monocyte subset in patients with AIDS dementia. The Lancet 349:692–695.

73. Ziegler-Heitbrock L. 2007. The CD14+ CD16+ blood monocytes: their role in infection and inflammation. Journal of Leukocyte Biology 81:584–592.

74. Veenstra M, León-Rivera R, Li M, Gama L, Clements JE, Berman JW. 2017. Mechanisms of CNS Viral Seeding by HIV $^{+}$ CD14 $^{+}$ CD16 $^{+}$ Monocytes: Establishment and Reseeding of Viral Reservoirs Contributing to HIV-Associated Neurocognitive Disorders. mBio 8:e01280-17.

75. Williams DW, Eugenin EA, Calderon TM, Berman JW. 2012. Monocyte maturation, HIV susceptibility, and transmigration across the blood brain barrier are critical in HIV neuropathogenesis. Journal of Leukocyte Biology 91:401–415.

76. Cayrol R, Wosik K, Berard JL, Dodelet-Devillers A, Ifergan I, Kebir H, Haqqani AS, Kreymborg K, Krug S, Moumdjian R, Bouthillier A, Becher B, Arbour N, David S, Stanimirovic D, Prat A. 2008. Activated leukocyte cell adhesion molecule promotes leukocyte trafficking into the central nervous system. Nat Immunol 9:137–145.

77. Martìn-Padura I, Lostaglio S, Schneemann M, Williams L, Romano M, Fruscella P, Panzeri C, Stoppacciaro A, Ruco L, Villa A, Simmons D, Dejana E. 1998. Junctional Adhesion Molecule, a Novel Member of the Immunoglobulin Superfamily That Distributes at Intercellular Junctions and Modulates Monocyte Transmigration. Journal of Cell Biology 142:117–127.

78. Muller WA, Weigl SA, Deng X, Phillips DM. 1993. PECAM-1 is required for transendothelial migration of leukocytes. Journal of Experimental Medicine 178:449–460.

79. Williams DW, Calderon TM, Lopez L, Carvallo-Torres L, Gaskill PJ, Eugenin EA, Morgello S, Berman JW. 2013. Mechanisms of HIV Entry into the CNS: Increased Sensitivity of HIV Infected CD14+CD16+ Monocytes to CCL2 and Key Roles of CCR2, JAM-A, and ALCAM in Diapedesis. PLoS ONE 8:e69270.

80. Kruize Z, Kootstra NA. 2019. The Role of Macrophages in HIV-1 Persistence and Pathogenesis. Front Microbiol 10:2828.

81. Meucci O, Fatatis A, Simen AA, Bushell TJ, Gray PW, Miller RJ. 1998. Chemokines regulate hippocampal neuronal signaling and gp120 neurotoxicity. Proc Natl Acad Sci USA 95:14500–14505.

82. Patel CA, Mukhtar M, Pomerantz RJ. 2000. Human Immunodeficiency Virus Type 1 Vpr Induces Apoptosis in Human Neuronal Cells. J Virol 74:9717–9726.

83. Piller SC, Jans P, Gage PW, Jans DA. 1998. Extracellular HIV-1 virus protein R causes a large inward current and cell death in cultured hippocampal neurons: Implications for AIDS pathology. Proc Natl Acad Sci USA 95:4595–4600.

84. Song L, Nath A, Geiger J, Moore A, Hochman S. 2003. Human Immunodeficiency Virus Type 1 Tat Protein Directly Activates Neuronal N -methyl- D -aspartate Receptors at an Allosteric Zinc-Sensitive Site. J Neurovirol 9:399–403.

85. Baxter EW, Graham AE, Re NA, Carr IM, Robinson JI, Mackie SL, Morgan AW. 2020. Standardized protocols for differentiation of THP-1 cells to macrophages with distinct M(IFNγ+LPS), M(IL-4) and M(IL-10) phenotypes. Journal of Immunological Methods 478:112721.

86. Smith M, Young H, Hurlstone A, Wellbrock C. 2015. Differentiation of THP1 Cells into Macrophages for Transwell Co-culture Assay with Melanoma Cells. BIO-PROTOCOL 5.

87. Sparks J. 2013. Role of HIV-1 Vpr on Host-Cellular Functions: Cell-Specific Analysis in Productively-Infected Macrophages. University of Pittsburgh Master's Thesis.

88. 2016. Tumor necrosis factor alfa, p. 230–232. *In* Meyler's Side Effects of Drugs. Elsevier.

89. Chanput W, Mes JJ, Wichers HJ. 2014. THP-1 cell line: An in vitro cell model for immune modulation approach. International Immunopharmacology 23:37–45.

90. Burdo TH, Lackner A, Williams KC. 2013. Monocyte/macrophages and their role in HIV neuropathogenesis. Immunol Rev 254:102–113.

91. Starr T, Bauler TJ, Malik-Kale P, Steele-Mortimer O. 2018. The phorbol 12-myristate-13-acetate differentiation protocol is critical to the interaction of THP-1 macrophages with Salmonella Typhimurium. PLoS ONE 13:e0193601.

92. Gatto F, Cagliani R, Catelani T, Guarnieri D, Moglianetti M, Pompa P, Bardi G. 2017. PMA-Induced THP-1 Macrophage Differentiation is Not Impaired by Citrate-Coated Platinum Nanoparticles. Nanomaterials 7:332.

93. Forrester MA, Wassall HJ, Hall LS, Cao H, Wilson HM, Barker RN, Vickers MA. 2018. Similarities and differences in surface receptor expression by THP-1 monocytes and differentiated macrophages polarized using seven different conditioning regimens. Cellular Immunology 332:58–76.

94. Aiken C. 1997. Pseudotyping human immunodeficiency virus type 1 (HIV-1) by the glycoprotein of vesicular stomatitis virus targets HIV-1 entry to an endocytic pathway and suppresses both the requirement for Nef and the sensitivity to cyclosporin A. J Virol 71:5871–5877.

95. Bol SM, Van Remmerden Y, Sietzema JG, Kootstra NA, Schuitemaker H, Van 'T Wout AB. 2009. Donor variation in in vitro HIV-1 susceptibility of monocyte-derived macrophages. Virology 390:205–211.

96. Yu D, Wang W, Yoder A, Spear M, Wu Y. 2009. The HIV Envelope but Not VSV Glycoprotein Is Capable of Mediating HIV Latent Infection of Resting CD4 T Cells. PLoS Pathog 5:e1000633.

97. Lodge R, Gilmore J, Ferreira Barbosa J, Lombard-Vadnais F, Cohen É. 2017. Regulation of CD4 Receptor and HIV-1 Entry by MicroRNAs-221 and -222 during Differentiation of THP-1 Cells. Viruses 10:13.

98. Tang S, Zhao J, Wang A, Viswanath R, Harma H, Little RF, Yarchoan R, Stramer SL, Nyambi PN, Lee S, Wood O, Wong EY, Wang X, Hewlett IK. 2010. Characterization of Immune Responses to Capsid Protein p24 of Human Immunodeficiency Virus Type 1 and Implications for Detection. Clin Vaccine Immunol 17:1244–1251.

99. Kumar A, Herbein G. 2014. The macrophage: a therapeutic target in HIV-1 infection. Mol and Cell Ther 2:10.

100. Koppensteiner H, Brack-Werner R, Schindler M. 2012. Macrophages and their relevance in Human Immunodeficiency Virus Type I infection. Retrovirology 9:82.

101. Müllers E. 2013. The Foamy Virus Gag Proteins: What Makes Them Different? Viruses 5:1023–1041.

102. Bell NM, Lever AML. 2013. HIV Gag polyprotein: processing and early viral particle assembly. Trends in Microbiology 21:136–144.

103. Fun A, Wensing AM, Verheyen J, Nijhuis M. 2012. Human Immunodeficiency Virus gag and protease: partners in resistance. Retrovirology 9:63.

104. Miura Y, Misawa N, Kawano Y, Okada H, Inagaki Y, Yamamoto N, Ito M, Yagita H, Okumura K, Mizusawa H, Koyanagi Y. 2003. Tumor necrosis factor-related apoptosis-

inducing ligand induces neuronal death in a murine model of HIV central nervous system infection. Proc Natl Acad Sci USA 100:2777–2782.

105. Brabers NACH, Nottet HSLM. 2006. Role of the pro-inflammatory cytokines TNF-alpha and IL-1beta in HIV-associated dementia. Eur J Clin Invest 36:447–458.

106. Mastroianni CM, Paoletti F, Valenti C, Vullo V, Jirillo E, Delia S. 1992. Tumour necrosis factor (TNF-alpha) and neurological disorders in HIV infection. Journal of Neurology, Neurosurgery & Psychiatry 55:219–221.

107. Liu X, Yin S, Chen Y, Wu Y, Zheng W, Dong H, Bai Y, Qin Y, Li J, Feng S, Zhao P. 2018. LPS-induced proinflammatory cytokine expression in human airway epithelial cells and macrophages via NF-κB, STAT3 or AP-1 activation. Mol Med Report https://doi.org/10.3892/mmr.2018.8542.

108. Bosshart H, Heinzelmann M. 2016. THP-1 cells as a model for human monocytes. Ann Transl Med 4:438–438.

109. Dos Reis RS, Sant S, Keeney H, Wagner MCE, Ayyavoo V. 2020. Modeling HIV-1 neuropathogenesis using three-dimensional human brain organoids (hBORGs) with HIV-1 infected microglia. Sci Rep 10:15209.